

Spatially Coupled PLDPC-Hadamard Convolutional Codes

Peng W. Zhang, Francis C.M. Lau, *Fellow, IEEE*,
and Chiu-W. Sham, *Senior Member, IEEE*

Abstract—We propose a new type of ultimate-Shannon-limit-approaching codes called spatially coupled protograph-based low-density parity-check Hadamard convolutional codes (SC-PLDPCH-CCs), which are constructed by spatially coupling PLDPC-Hadamard block codes. We develop an efficient decoding algorithm that combines pipeline decoding and layered scheduling for the decoding of SC-PLDPCH-CCs, and analyze the latency and complexity of the decoder. To estimate the decoding thresholds of SC-PLDPCH-CCs, we first propose a layered protograph extrinsic information transfer (PEXIT) algorithm to evaluate the thresholds of spatially coupled PLDPC-Hadamard terminated codes (SC-PLDPCH-TDCs) with a moderate coupling length. With the use of the proposed layered PEXIT method, we develop a genetic algorithm to find good SC-PLDPCH-TDCs in a systematic way. Then we extend the coupling length of these SC-PLDPCH-TDCs to form good SC-PLDPCH-CCs. Results show that our constructed SC-PLDPCH-CCs can achieve comparable thresholds to the block code counterparts. Simulations illustrate the superiority of the SC-PLDPCH-CCs over the block code counterparts and other state-of-the-art low-rate codes in terms of error performance. For the rate-0.00295 SC-PLDPCH-CC, a bit error rate of 10^{-5} is achieved at $E_b/N_0 = -1.465$ dB, which is only 0.125 dB from the ultimate Shannon limit.

Index Terms—Protograph LDPC code, PLDPC-Hadamard code, PEXIT algorithm, spatially coupled PLDPC codes, spatially coupled PLDPC Hadamard codes, ultimate Shannon limit.

I. INTRODUCTION

P. W. Zhang was with the Future Wireless Networks and IoT Focusing Area, Department of Electronic and Information Engineering, The Hong Kong Polytechnic University, Hong Kong SAR, China. He is now with Huawei Technologies Ltd., Chengdu, China.

F. C. M. Lau is with the Future Wireless Networks and IoT Focusing Area, Department of Electronic and Information Engineering, The Hong Kong Polytechnic University, Hong Kong SAR, China. (e-mail: francis-cm.lau@polyu.edu.hk).

C.-W. Sham is with the Department of Computer Science, The University of Auckland, New Zealand (e-mail: b.sham@auckland.ac.nz).

The work described in this paper was partially supported by the RGC Research Impact Fund from the Hong Kong SAR, China (Project No. R5013-19).

Binary low-density parity-check (LDPC) codes were first proposed in 1963 [1], whose sparse parity-check matrix containing “0” and “1” is randomly constructed, and can be graphically represented by a Tanner graph [2]. A Tanner graph consists of check nodes (CNs), variable nodes (VNs) and the connections between CNs and VNs. After receiving the channel observations, extrinsic information along the connections is iteratively exchanged and calculated at CN processors and VN processors to realize belief propagation (BP) decoding. In [3], a density evolution method is proposed to evaluate the probability density function (PDF) of the extrinsic information and hence to optimize the degree distributions of LDPC codes. Subsequently in [4], an extrinsic information transfer (EXIT) chart technique is proposed to optimize LDPC codes by calculating the mutual information (MI) of the extrinsic information. Through both methods, good-performing LDPC codes are constructed to work close to the Shannon limit under binary erasure channels (BECs), binary symmetric channels (BSCs) and additive-white-Gaussian-noise (AWGN) channels [3], [4], [5]. Yet, most LDPC codes are designed to achieve good decoding performance at a bit-energy-to-noise-power-spectral-density ratio (E_b/N_0) greater than 0 dB. To approach the ultimate Shannon limit, i.e., $E_b/N_0 = -1.59$ dB [6], other low-rate codes are designed. Potential application scenarios of such codes include multiple access wireless systems (e.g., interleaved-division multiple-access [7], [8] with a huge number of non-orthogonal users) and deep space communications. In [9] and [10], very low-rate turbo Hadamard codes and zigzag Hadamard codes are proposed. However, their decoders require the use of serial decoding [11], [12], [13] and cannot make use of parallel decoding as in LDPC decoders. The error performances of turbo Hadamard codes and zigzag Hadamard codes are also not as good as those of the

LDPC-Hadamard codes that have been subsequently proposed [14].

In the Tanner graph of an LDPC code, the edges connected to a VN form a repeat code, whereas the edges connected to a CN form a single-parity-check (SPC) code. When the repeat codes and/or SPC codes are replaced with other block codes, a Tanner graph of a generalized LDPC is formed. By replacing SPC codes with Hadamard codes, LDPC-Hadamard codes (LDPC-HCs) have been proposed and their degree distributions have been optimized with the EXIT chart method [14]. The LDPC-HCs not only have thresholds lower than -1.34 dB, but also achieve excellent decoding performance at a E_b/N_0 lower than -1.17 dB. On the other hand, the EXIT chart method cannot effectively analyze degree distributions containing degree-1 and/or punctured VNs. The parity-check matrix derived by the progressive-edge-growth (PEG) method [15] according to the degree distributions does not contain any structure and therefore does not facilitate linear encoding and parallel decoding. In [16], a class of structured LDPC-HCs called protograph-based LDPC-HCs (PLDPC-HCs) have been proposed.

Protoph-graph-based LDPC (PLDPC) codes can be described by a small protomatrix or protograph [17]. Using the copy-and-permute operations to lift the protomatrix or protograph, the derived matrix or lifted graph can easily have a quasi-cyclic structure which is conducive to the hardware implementations of encoders and decoders [18]. PLDPC-HCs [16] also inherit such advantages from PLDPC codes. By adding an appropriate amount of degree-1 Hadamard variable nodes (D1H-VNs) to the check nodes in the protograph of a PLDPC code, the SPC constraints are converted into Hadamard constraints and the protograph of a PLDPC-HC is obtained. The protograph-based EXIT (PEXIT) chart method for PLDPC codes [19] has further been modified for analyzing PLDPC-HCs [16]. The modified method not only can produce multiple extrinsic mutual information from the symbol-by-symbol maximum-a-posteriori-probability (symbol-MAP) Hadamard decoder, but also is applicable to analyzing protographs with degree-1 and/or punctured VNs. The structured PLDPC-HCs can achieve good thresholds and comparable error performance as the traditional LDPC-HCs. In [20], a layered decoding algorithm has been proposed to double the convergence rate compared with standard decoding.

While PLDPC-HCs are already working very close to the ultimate Shannon limit, further improvement is possible. In [21], it has been shown that LDPC convolutional codes (LDPC-CCs) can achieve convolutional gains over their block-code counterparts. LDPC-CCs were first proposed in [22] and characterized by the degree distributions of the underlying LDPC block codes (LDPC-BCs). In addition, spatially coupled LDPC (SC-LDPC) codes are constructed by coupling a number of LDPC-BCs. As the number of coupled LDPC-BCs tends to infinity, spatially coupled LDPC convolutional codes (SC-LDPC-CCs) are obtained. In [23] and [24], SC-LDPC-CCs have been shown to achieve capacity over binary memoryless symmetric channels under BP decoding. In [25], SC-LDPC-CCs have been constructed from the perspective of protographs, namely SC-PLDPC-CCs. Through the edge-spreading procedure on protomatrix, the threshold, convergence behavior and error performance of SC-PLDPC ensembles have also been systematically investigated. In particular, PEXIT algorithms have been applied to analyze binary [26] and q -ary SC-LDPC codes [27]. Based on the aforementioned results, spatially coupled PLDPC-Hadamard convolutional codes (SC-PLDPCH-CCs), which are to be investigated in this paper, have the potential to provide extra gains over their block-code counterparts. A genetic algorithm (GA) will also be proposed to optimize the design of SC-PLDPCH-CCs.

GA is an optimization algorithm that simulates the evolution of nature, and is widely used in music generation, genetic synthesis and VLSI technology [28]. In the arena of channel codes, GA has been applied to adjust the code rate of turbo codes without puncturing [29]; to construct polar codes that reduce the decoding complexity while maintaining the same decoding performance [30]; together with bit-error-rate (BER) simulations to optimize error performance of short length LDPC codes over both AWGN and Rayleigh fading channels [31]; together with density evolution to optimize the degree distributions of the SC-LDPC codes over BEC channels [32]. GA first forms an offspring generation from the parent generation, and performs operations such as crossover, mutation, and selection on the offspring generation. A similar technique called differential evolution algorithm directly uses the parent generation to perform these operations to

achieve the evolution. Differential evolution based optimization methods have been applied to design LDPC and SC-LDPC codes [33], [34]. Compared with the differential evolution algorithm, the genetic algorithm has a stronger global search ability but requires more complex procedures.

In this paper we propose a new type of ultimate-Shannon-limit-approaching codes, namely spatially coupled PLDPC-Hadamard convolutional codes (SC-PLDPCH-CCs), and we conduct an in-depth investigation into the proposed codes. Our main contributions are as follows.

- 1) We propose a new type of ultimate-Shannon-limit-approaching codes, namely spatially coupled PLDPC-Hadamard convolutional codes (SC-PLDPCH-CCs), which are constructed by spatially coupling PLDPC-Hadamard block codes.
- 2) We describe the encoding method of SC-PLDPCH-CCs. We also develop an efficient decoding algorithm, i.e., a pipeline decoding strategy combined with layered scheduling, for the decoding of SC-PLDPCH-CCs, and analyze its latency and complexity.
- 3) Using the original PEXIT method in [16], we show that the thresholds of different spatially coupled PLDPC-Hadamard terminated codes (SC-PLDPCH-TDCs) are distinguishable and improves as the coupling length increases. To improve the convergence rate of the original PEXIT method, we propose a layered PEXIT algorithm to efficiently evaluate the threshold of SC-PLDPCH-TDCs with a given coupling length. The thresholds of SC-PLDPCH-TDCs with large coupling lengths are then used as estimates for thresholds of SC-PLDPCH-CCs.
- 4) We propose a GA to systematically search for SC-PLDPCH-TDCs having good thresholds. Based on the same set of split protomatrices for good SC-PLDPCH-TDCs, we extend the coupling length to construct the convolutional codes, i.e., SC-PLDPCH-CCs.
- 5) We have found SC-PLDPCH-CCs with comparable thresholds to the underlying PLDPC-Hadamard block codes (PLDPCH-BCs). Simulation results show that SC-PLDPCH-CCs outperform their PLDPCH-BC counterparts and other state-of-the-art low-rate codes in terms of bit error performance. For the rate-0.00295 SC-PLDPCH-CC, a BER of 10^{-5} is achieved

at $E_b/N_0 = -1.465$ dB.

Section II of this paper highlights the main differences/improvements of the current work compared with the previously studied PLDPC-HCs. Section III reviews the structures of related block codes and spatially coupled codes. Section IV introduces the structure and encoding process of SC-PLDPCH-CCs; describes a pipeline decoding strategy combined with layered scheduling for decoding SC-PLDPCH-CCs, and analyzes its latency and complexity. Also, a layered PEXIT chart method is proposed to evaluate the threshold of SC-PLDPCH-TDCs/SC-PLDPCH-CCs efficiently and a GA is proposed to optimize protomatrices for SC-PLDPCH-TDCs/SC-PLDPCH-CCs. Section V presents the thresholds and optimized protomatrices of SC-PLDPCH-CCs with different code rates. It also compares the simulated BER results of the SC-PLDPCH-CCs with those of the underlying protograph-based PLDPC-Hadamard block codes (PLDPCH-BCs) and other state-of-the-art low-rate codes. Finally, Section VI presents some concluding remarks.

II. MAIN DIFFERENCES/IMPROVEMENTS BETWEEN THIS WORK AND PREVIOUS WORKS

The major differences/improvements between the current work and the previously studied PLDPC-HCs [16], [20] are as follows.

- 1) The PLDPC-HCs in [16], [20] and the codes being investigated in this work are constructed based on protographs with the SPC check nodes (SPC-CN) replaced by Hadamard constraints. However, the PLDPC-HCs studied in [16], [20] are block codes while the codes being investigated in this work are formed by spatially coupling these block codes.
- 2) Though PEXIT algorithms have been applied for analyzing the codes in [16] and in this work, a layered PEXIT algorithm is proposed in this work to improve the convergence rate of the original PEXIT algorithm in [16]. Also, a more efficient way of evaluating the extrinsic MI of the Hadamard CNs is applied in the algorithm here compared with [16].
- 3) A GA is proposed in this work to search for spatially-coupled PLDPC-HCs with good theoretical thresholds.

- 4) We estimate the thresholds of SC-PLDPCH-CCs based on the thresholds of SC-PLDPCH-TDCs with large coupling lengths.
- 5) The PLDPC-Hadamard sub-decoders in [20] and the processors in this work are of similar structures. All of them apply layered decoding algorithms for decoding the PLDPC-HCs. However, the structure of the PLDPC-Hadamard sub-decoders in [20] is more or less fixed for a given code design; and the number of decoding iterations affects the error performance of the code, the decoding latency and throughput. The pipeline decoder described in this work consists of a series of processors, the number of which can vary; and the number of processors in the decoder affects the error performance of the code, the decoding latency, the hardware complexity and throughput.
- 6) The SC-PLDPCH-CCs in this work can achieve a better error performance and throughput than the PLDPCH-BCs [16] with a higher hardware requirement.

III. BACKGROUND

A. PLDPC Block Codes

A protograph consists of a set of m SPC-CN, a set of n ($n > m$) protograph variable nodes (P-VNs), and a set of edges connecting the SPC-CN to the P-VNs [17]. The corresponding protomatrix can be denoted by $\mathbf{B} = \{b(i, j)\}$ in which each row in \mathbf{B} corresponds to a SPC-CN; each column corresponds to a P-VN; and $b(i, j)$ corresponds to the number of edges connecting the i -th SPC-CN and the j -th P-VN. The code rate of a PLDPC block code equals $R_{\text{PLDPC-BC}} = 1 - \frac{m}{n}$. A two-step lifting method (with factors z_1 and z_2) can be used to lift the protomatrix and hence to construct the parity-check matrix of a PLDPC code [35]. After the first lifting, all entries in the lifted matrix are either “0” or “1”. The second lifting procedure aims to construct a parity-check matrix with a quasi-cyclic structure so as to simplify encoder and decoder designs.

B. LDPC-Hadamard Codes and PLDPC-Hadamard Codes

A Hadamard code with an order r has a code length of $q = 2^r$ and can be obtained by a Hadamard

matrix \mathbf{H}_q of size $q \times q$. \mathbf{H}_q can be recursively generated using [9], [14] $\pm \mathbf{H}_q = \pm \{\mathbf{h}_j\} = \begin{bmatrix} \pm \mathbf{H}_{q/2} & \pm \mathbf{H}_{q/2} \\ \pm \mathbf{H}_{q/2} & \mp \mathbf{H}_{q/2} \end{bmatrix}$ where $\pm \mathbf{H}_1 = [\pm 1]$; $\pm \mathbf{h}_j = [\pm h_{0,j} \pm h_{1,j} \cdots \pm h_{2^r-1,j}]^T$ ($j = 0, 1, \dots, q-1$) represents the j -th column of $\pm \mathbf{H}_q$ and is a Hadamard codeword. Suppose +1 is mapped to bit “0” and −1 to bit “1”. It has been shown that when the Hadamard order r is an even number, the 0th, 1st, 2nd, \dots , 2^{k-1} -th, \dots , 2^{r-1} -th, and $(2^r - 1)$ -th code bits (total $r + 2$ bits) in each codeword $\pm \mathbf{h}_j$ satisfy the SPC constraint together, i.e., [14], [16]

$$[\pm h_{0,j} \oplus \pm h_{1,j} \oplus \cdots \oplus \pm h_{2^{k-1},j} \oplus \cdots \oplus \pm h_{2^{r-1},j}] \oplus \pm h_{2^r-1,j} = 0, \quad (1)$$

where the symbol \oplus represents the XOR operator. When the SPC codes of an LDPC code are replaced with Hadamard block codes with additional Hadamard parity-check bits, an LDPC-Hadamard block code (LDPCH-BC) is formed [14]. LDPCH-BCs can be constructed by lifting protographs in which the SPC-CN have been replaced with Hadamard check nodes (H-CN) and additional parity-check bits. Such LDPCH-BCs are called PLDPCH-BCs [16]. We assume that each SPC-CN in the original protograph connects d P-VNs. The corresponding d bit values can be used as information bits and input to a systematic Hadamard encoder with an order r , where $r = d - 2$. When r is an even number, these $d = r + 2$ inputs correspond to those entries in (1), based on which the remaining $2^r - d$ Hadamard parity-check bits (represented by D1H-VNs in the protograph) are found.¹ Fig. 1(a) illustrates the protograph of a PLDPCH-BC consisting of $m = 3$ H-CN and $n = 4$ P-VNs. Using a two-step lifting process with factors z_1 and z_2 , a PLDPCH-BC can be constructed with an information length of $(n - m)z_1z_2$. When r is even, the overall code length equals $nz_1z_2 + m(2^r - r - 2)z_1z_2$ [16] and the code rate of the PLDPCH-BC is given by $R_{\text{PLDPCH-BC}}^{\text{even}} = \frac{n-m}{n+m(2^r-r-2)}$.

C. Spatially Coupled LDPC Codes

1) *LDPC convolutional codes*: The parity-check matrix \mathbf{H}_{CC} of an LDPC-CC [22] is semi-infinite

¹When r is an odd number, the Hadamard code bits do not satisfy (1). Thus, a non-systematic Hadamard encoding scheme is used and $2^r - 2$ Hadamard parity-check bits are generated [16]. Here, we focus our analysis on cases where r is even.

and structurally repeated. \mathbf{H}_{CC} can be written as in (2), where each $\mathbf{H}_i(t)$ ($i = 0, 1, \dots, m_s$) is an $M \times N$ component parity-check matrix, t denotes the time index, and m_s is the syndrome former memory. Each codeword \mathbf{c} satisfies $\mathbf{c}\mathbf{H}_{CC}^T = \mathbf{0}$, where $\mathbf{0}$ is a semi-infinite zero vector.

2) *Spatially coupled PLDPC codes*: SC-PLDPC codes are constructed based on underlying PLDPC block codes (PLDPC-BCs). We denote W as the coupling width (equivalent to the aforementioned syndrome former memory m_s) and L as the coupling length. Based on the $m \times n$ protomatrix \mathbf{B} of an underlying PLDPC-BC, an edge-spreading procedure [36] can be first used to obtain $W + 1$ split protomatrices \mathbf{B}_i ($i = 0, 1, \dots, W$) under the constraint $\mathbf{B} = \sum_{i=0}^W \mathbf{B}_i$. Then L sets of such protomatrices are coupled to construct an SC-PLDPC code [25]. When the L sets of protomatrices are coupled and directly terminated, the resultant protomatrix equals (3). Such code is called an SC-PLDPC terminated code (SC-PLDPC-TDC) and its code rate equals $R_{SC-PLDPC-TDC} = 1 - \frac{L+W}{L}(1 - R_{PLDPC-BC})$ where $R_{PLDPC-BC} = 1 - \frac{m}{n}$ is the code rate of its underlying block code. When the protograph of a spatially coupled code is terminated with “end-to-end” connections, the corresponding code is called SC-PLDPC tail-biting code (SC-PLDPC-TBC), whose protomatrix can be written as (4). The code rate $R_{SC-PLDPC-TBC}$ of an SC-PLDPC-TBC is the same as that of its underlying block code, i.e., $R_{SC-PLDPC-TBC} = \frac{nL-mL}{nL} = R_{PLDPC-BC}$. By extending the coupling length L of an SC-PLDPC-TDC to infinity, an SC-PLDPC-CC is formed. The semi-infinite protomatrix of an SC-PLDPC-CC is given by (5). The code rate of SC-PLDPC-CC equals that of the underlying block code [25], i.e., $R_{SC-PLDPC-CC} = \lim_{L \rightarrow \infty} R_{SC-PLDPC-TDC} = R_{PLDPC-BC}$. Once the protomatrix of a spatially coupled code is derived, a two-step lifting method can be used to construct a SC-PLDPC code. (A single-step lifting method [37] can also be used to obtain an SC-PLDPC code.)

IV. SPATIALLY COUPLED PLDPC-HADAMARD CONVOLUTIONAL CODES

In this section, we show the details of our proposed SC-PLDPCH-CC. First, we show the way of constructing SC-PLDPCH codes, including SC-PLDPCH tail-biting code (SC-PLDPCH-TBC), SC-PLDPCH terminated code (SC-PLDPCH-TDC) and

SC-PLDPCH-CC, from its block code counterpart. Second, we briefly explain the encoding process of SC-PLDPCH-CCs. Third, we describe an efficient decoding algorithm for SC-PLDPCH-CC, which combines the layered decoding used for decoding PLDPCH-BC [20] and the pipeline decoding used for decoding SC-PLDPC-CC [38]. Fourth, we propose a layered PEXIT algorithm for evaluating the theoretical threshold of an SC-PLDPCH-TDC, which is then used to approximate the threshold of the corresponding SC-PLDPCH-CC. Fifth, we propose a GA to optimize the SC-PLDPCH-TDC/SC-PLDPCH-CC designs based on a given PLDPCH-BC.

A. Code Construction

SC-PLDPCH codes are constructed in a similar way as SC-PLDPC codes. We also denote the coupling width as W and coupling length as L in an SC-PLDPCH code. Given a PLDPCH-BC with a protomatrix \mathbf{B} , we apply the edge-spreading procedure to split \mathbf{B} into $W + 1$ protomatrices \mathbf{B}_i ($i = 0, 1, \dots, W$) under the constraint $\mathbf{B} = \sum_{i=0}^W \mathbf{B}_i$. Then we couple L sets of these matrices to construct the protomatrix of a SC-PLDPCH code. Similar to the SC-PLDPC codes described in Section III-C, an SC-PLDPCH-TDC is formed if the coupled matrices are directly terminated; an SC-PLDPCH-TBC is formed if the coupled matrices are connected end-to-end; and an SC-PLDPCH-CC is formed if the coupling length L becomes infinite. Since the constructed protomatrices only represent the connections between P-VNs and H-CNns, SC-PLDPCH codes have protomatrix structures similar to those of SC-PLDPC codes, i.e., (3) for SC-PLDPCH-TDC; (4) for SC-PLDPCH-TBC; and (5) for SC-PLDPCH-CC. Unlike the protographs of SC-PLDPC codes which consist of P-VNs and SPC-CNns, the protographs of SC-PLDPCH codes contain P-VNs and H-CNns connected with some appropriate D1H-VNs. Fig. 1(b) shows the protograph of an SC-PLDPCH-CC derived from the PLDPCH-BC in Fig. 1(a). SC-PLDPCH codes can be constructed from the coupled protographs using the lifting process. Assuming that \mathbf{B} has a constant row weight of d and hence an order- r ($= d - 2$) Hadamard code is used (recall r is even), it can be readily shown that the code rates of the SC-PLDPCH codes are as follows. For SC-PLDPCH-TDCs the code rate

$$\mathbf{H}_{\text{CC}} = \begin{bmatrix} \mathbf{H}_0(1) \\ \mathbf{H}_1(1) & \mathbf{H}_0(2) \\ \vdots & \mathbf{H}_1(2) & \ddots \\ \mathbf{H}_{m_s}(1) & \vdots & \ddots & \mathbf{H}_0(t) \\ & \mathbf{H}_{m_s}(2) & \ddots & \mathbf{H}_1(t) & \ddots \\ & & \ddots & \vdots & \ddots \\ & & & \mathbf{H}_{m_s}(t) & \ddots \\ & & & & \ddots \end{bmatrix} \quad (2)$$

$$\mathbf{B}_{\text{SC-PLDPC-TDC}} = \left[\begin{array}{cccc} \overbrace{\begin{bmatrix} \mathbf{B}_0 \\ \mathbf{B}_1 & \mathbf{B}_0 \\ \vdots & \mathbf{B}_1 & \ddots \\ \mathbf{B}_W & \vdots & \ddots & \mathbf{B}_0 \\ & \mathbf{B}_W & \ddots & \mathbf{B}_1 \\ & & \ddots & \vdots \\ & & & \mathbf{B}_W \end{bmatrix}}^{nL} \end{array} \right] \left. \vphantom{\begin{bmatrix} \mathbf{B}_0 \\ \mathbf{B}_1 & \mathbf{B}_0 \\ \vdots & \mathbf{B}_1 & \ddots \\ \mathbf{B}_W & \vdots & \ddots & \mathbf{B}_0 \\ & \mathbf{B}_W & \ddots & \mathbf{B}_1 \\ & & \ddots & \vdots \\ & & & \mathbf{B}_W \end{bmatrix}} \right\} m(L+W). \quad (3)$$

$$\mathbf{B}_{\text{SC-PLDPC-TBC}} = \left[\begin{array}{cccc} \overbrace{\begin{bmatrix} \mathbf{B}_0 & & & \mathbf{B}_W & \cdots & \mathbf{B}_1 \\ \mathbf{B}_1 & \mathbf{B}_0 & & & & \vdots \\ \vdots & \mathbf{B}_1 & \mathbf{B}_0 & & & \mathbf{B}_W \\ \mathbf{B}_W & \vdots & \mathbf{B}_1 & \ddots & & \\ & \mathbf{B}_W & \vdots & \ddots & \mathbf{B}_0 & \\ & & \mathbf{B}_W & \ddots & \mathbf{B}_1 & \mathbf{B}_0 \\ & & & \ddots & \vdots & \mathbf{B}_0 \\ & & & & \mathbf{B}_W & \cdots & \mathbf{B}_1 & \mathbf{B}_0 \end{bmatrix}}^{nL} \end{array} \right] \left. \vphantom{\begin{bmatrix} \mathbf{B}_0 & & & \mathbf{B}_W & \cdots & \mathbf{B}_1 \\ \mathbf{B}_1 & \mathbf{B}_0 & & & & \vdots \\ \vdots & \mathbf{B}_1 & \mathbf{B}_0 & & & \mathbf{B}_W \\ \mathbf{B}_W & \vdots & \mathbf{B}_1 & \ddots & & \\ & \mathbf{B}_W & \vdots & \ddots & \mathbf{B}_0 & \\ & & \mathbf{B}_W & \ddots & \mathbf{B}_1 & \mathbf{B}_0 \\ & & & \ddots & \vdots & \mathbf{B}_0 \\ & & & & \mathbf{B}_W & \cdots & \mathbf{B}_1 & \mathbf{B}_0 \end{bmatrix}} \right\} mL \quad (4)$$

$$\mathbf{B}_{\text{SC-PLDPC-CC}} = \begin{bmatrix} \mathbf{B}_0 \\ \mathbf{B}_1 & \mathbf{B}_0 \\ \vdots & \mathbf{B}_1 & \ddots \\ \mathbf{B}_W & \vdots & \ddots & \mathbf{B}_0 \\ & \mathbf{B}_W & \ddots & \mathbf{B}_1 & \ddots \\ & & \ddots & \vdots & \ddots \\ & & & \mathbf{B}_W & \ddots \\ & & & & \ddots \end{bmatrix}. \quad (5)$$

equals $R_{\text{SC-PLDPCH-TDC}}^{\text{even}} = \frac{nL-m(L+W)}{nL+m(L+W)(2^r-d)} = \frac{n-m(1+\frac{W}{L})}{n+m(1+\frac{W}{L})(2^r-d)}$. For SC-PLDPCH-TBCs and SC-PLDPCH-CCs, their code rates are the same as the block code counterparts, i.e., $R_{\text{SC-PLDPCH-TBC}}^{\text{even}} = R_{\text{SC-PLDPCH-CC}}^{\text{even}} = R_{\text{PLDPCH-BC}}^{\text{even}} = \frac{n-m}{n+m(2^r-r-2)}$.

B. Encoding of SC-PLDPCH-CC

From this point forward and unless otherwise stated, we focus our study on SC-PLDPCH-CC. We also assume that the row weight of \mathbf{B} equals $d = r + 2$ and is even. After performing a two-step lifting process on (5), we obtain the semi-infinite parity-check matrix of an SC-PLDPCH-CC in Fig. 2. Denoting the two lifting factors by z_1 and z_2 , each \mathbf{H}_i ($i = 0, 1, \dots, W$) which is the lifted \mathbf{B}_i has a size of $M \times N = mz_1z_2 \times nz_1z_2$. At time t , $M - N$ information bits denoted by $\mathbf{b}(t) \in \{0, 1\}^{M-N}$ are input to the SC-PLDPCH-CC encoder. The output of the SC-PLDPCH-CC encoder contains N coded bits corresponding to P-VNs, which are denoted by $\mathbf{P}(t)$; and $M(2^r - r - 2)$ Hadamard parity-check bits corresponding to D1H-VNs, which are denoted by $\mathbf{D}(t)$. Referring to Fig. 2, we generate the output bits as follows.

- 1) $t = 1$: Given $\mathbf{b}(1)$, $\mathbf{P}(1)$ is generated based on the first block row of $\mathbf{H}_{\text{SC-PLDPCH-CC}}$, i.e., \mathbf{H}_0 . Moreover, $\mathbf{D}(1)$ is computed based on $\overbrace{[\mathbf{0} \cdots \mathbf{0}]}^W \mathbf{P}(1)$ and the structure $[\mathbf{H}_W \cdots \mathbf{H}_1 \mathbf{H}_0]$, where $\mathbf{0}$ is the length- N zero vector.
- 2) $t = 2$: Given $\mathbf{b}(2)$ and $\mathbf{P}(1)$, $\mathbf{P}(2)$ is generated based on the second block row of $\mathbf{H}_{\text{SC-PLDPCH-CC}}$, i.e., $[\mathbf{H}_1 \mathbf{H}_0]$. Moreover, $\mathbf{D}(2)$ is computed based on $\overbrace{[\mathbf{0} \cdots \mathbf{0}]}^{W-1} \mathbf{P}(1) \mathbf{P}(2)$ and the structure $[\mathbf{H}_W \cdots \mathbf{H}_1 \mathbf{H}_0]$.
- 3) $t \leq W$: Given $\mathbf{b}(t)$ and $[\mathbf{P}(1) \mathbf{P}(2) \cdots \mathbf{P}(t-1)]$, N coded bits $\mathbf{P}(t)$ are generated based on the t -th block row of $\mathbf{H}_{\text{SC-PLDPCH-CC}}$, i.e., $[\mathbf{H}_{t-1} \cdots \mathbf{H}_1 \mathbf{H}_0]$. $\mathbf{D}(t)$ corresponding to the $M(2^r - r - 2)$ D1H-VNs are computed based on $\overbrace{[\mathbf{0} \cdots \mathbf{0}]}^{W+1-t} \mathbf{P}(1) \cdots \mathbf{P}(t)$ and the structure $[\mathbf{H}_W \cdots \mathbf{H}_1 \mathbf{H}_0]$.
- 4) $t > W$: Given $\mathbf{b}(t)$ and $[\mathbf{P}(t-W) \mathbf{P}(t-W+1) \cdots \mathbf{P}(t-1)]$, $\mathbf{P}(t)$ is generated based on the t -th block row of $\mathbf{H}_{\text{SC-PLDPCH-CC}}$, i.e.,

$[\mathbf{H}_W \cdots \mathbf{H}_1 \mathbf{H}_0]$. Then, $\mathbf{D}(t)$ is computed based on $[\mathbf{P}(t-W) \cdots \mathbf{P}(t-1) \mathbf{P}(t)]$ and the structure $[\mathbf{H}_W \cdots \mathbf{H}_1 \mathbf{H}_0]$. The constraint length of the SC-PLDPCH-CC therefore equals $(W+1)N + M(2^r - r - 2)$.

Remarks: The values of $\mathbf{D}(t)$ are generated during the encoding corresponding to the t -th block row. They are not needed for generating other $\mathbf{D}(t')$ where $t \neq t'$. When $t \leq W$, $W+1-t$ length- N zero vectors are inserted in front of $\mathbf{P}(1)$ for computing $\mathbf{D}(t)$. But these zero vectors are not transmitted through the channel.

C. Pipeline Decoding

1) *Decoding Structure:* At the receiving end, we receive channel observations regarding the coded bits $\mathbf{P}(t)$ (corresponding to P-VNs) and Hadamard parity-check bits $\mathbf{D}(t)$ (corresponding to D1H-VNs). We denote the log-likelihood-ratio (LLR) values corresponding to $\mathbf{P}(t)$ by $\mathbf{L}_{ch}^P(t)$ and the LLR values corresponding to $\mathbf{D}(t)$ by $\mathbf{L}_{ch}^D(t)$. We consider a pipeline decoder which consists of I identical message-passing processors [22], [39], [38]. Each processor is a PLDPC-Hadamard block sub-decoder corresponding to $[\mathbf{H}_W \cdots \mathbf{H}_1 \mathbf{H}_0]$. Thus, each processor operates on $W+1$ sets of P-VNs and one set of D1H-VNs each time, i.e., a total of $N(W+1)$ P-VNs and $M(2^r - r - 2)$ D1H-VNs (when r is even). Hence the pipeline decoder operates on $(W+1)I$ sets of P-VNs and I sets of D1H-VNs each time. Each processor (sub-decoder) can apply either the standard decoding algorithm or the layered decoding algorithm to compute/update the *a posteriori* probability in LLR form (APP-LLR) for the coded bits $\mathbf{P}(t)$ and the related extrinsic LLR information. Here, we apply the layered decoding algorithm [20] in each of these PLDPC-Hadamard block sub-decoders.

We denote the APP-LLR values of the coded bits $\mathbf{P}(t)$ by $\mathbf{L}_{app}^P(t)$. Referring to Fig. 3, $\{\mathbf{L}_{ch}^P(1), \mathbf{L}_{ch}^D(1)\}$ is first input to the pipeline decoder and Processor #1 updates the APP-LLR of all P-VNs inside, i.e., $\mathbf{L}_{app}^P(1)$. Also, extrinsic LLR information is updated and stored in the processor but is not depicted in the figure. Then, $\{\mathbf{L}_{ch}^P(2), \mathbf{L}_{ch}^D(2)\}$ is input to the pipeline decoder while $\{\mathbf{L}_{ch}^P(1), \mathbf{L}_{ch}^D(1), \mathbf{L}_{app}^P(1)\}$ and related extrinsic LLR information are shifted to the left in the decoder. Processor #1 updates the APP-LLRs of

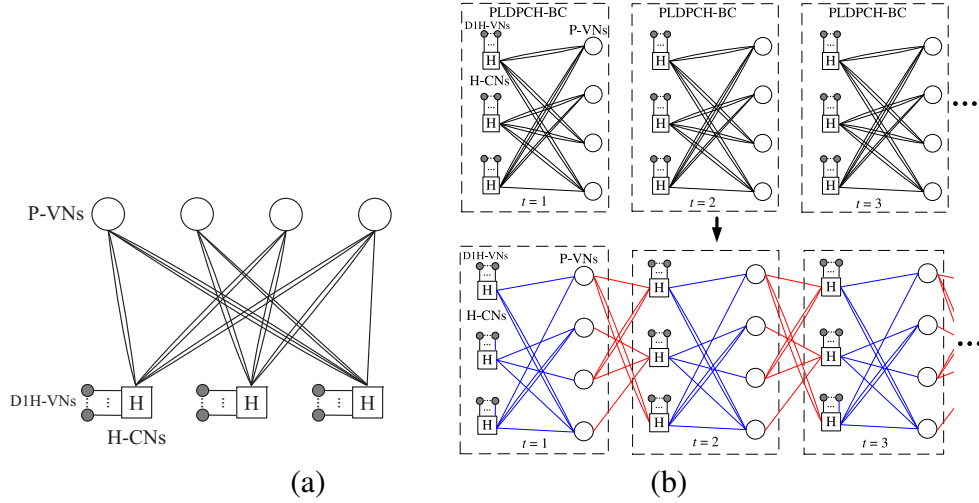


Fig. 1. (a) A protograph of PLDPC-Hadamard code. Number of D1H-VNs connected to each HCN is $2^r - d = 10$ using order- $r = d - 2 = 4$ Hadamard code. (b) Protograph of an SC-PLDPCH-CC derived from the PLDPC-Hadamard code.

$$\begin{aligned}
 &\text{Coded bits of P-VNs} \quad \{P(1), P(2), \dots, P(t-1), P(t), \dots\} \\
 &\text{Coded bits of D1H-VNs} \quad \{D(1), D(2), \dots, D(t-1), D(t), \dots\} \\
 \\
 &H_{\text{SC-PLDPCH-CC}} = \begin{bmatrix} H_0 & & & & \\ H_1 & H_0 & & & \\ \vdots & H_1 & \ddots & & \\ H_W & \vdots & \ddots & H_0 & \\ & H_W & \ddots & H_1 & H_0 \\ & & \ddots & \vdots & H_1 \\ & & & H_W & \vdots \\ & & & & H_W \end{bmatrix}
 \end{aligned}$$

Fig. 2. Encoding of an SC-PLDPCH-CC. Coded bits $P(1), P(2), \dots, P(t-1), P(t), \dots$ correspond to P-VNs at time $1, 2, \dots, t-1, t, \dots$. Hadamard parity-check bits $D(1), D(2), \dots, D(t-1), D(t), \dots$ correspond to D1H-VNs at time $1, 2, \dots, t-1, t, \dots$.

all P-VNs inside, i.e., $L_{app}^P(1)$ and $L_{app}^P(2)$. Again, extrinsic LLR information is updated and stored in the processor but is not depicted. Subsequently, $\{L_{ch}^P(t), L_{ch}^D(t)\}$ ($t = 3, 4, \dots$) are input into the decoder one set by one set. Every time, all sets of LLRs inside the decoder are shifted to the left by one “ H_i ” block, and all APP-LLRs of all P-VNs inside the different I processors are updated. When $\{L_{ch}^P((W+1)I+1), L_{ch}^D((W+1)I+1)\}$ is input to the pipeline decoder, the APP-LLRs $L_{app}^P(1)$ have gone through the iterative process and are output from the decoder. Hard decisions are made based on these APP-LLRs to determine the values of the coded bits $P(1)$. The process continues and every

time $\{L_{ch}^P((W+1)I+t'), L_{ch}^D((W+1)I+t')\}$ ($t' = 1, 2, \dots$) is input to the decoder, the APP-LLRs $L_{app}^P(t')$ are output and the values of the coded bits $P(t')$ are determined.

2) *Latency and Complexity Analysis:* In this section, we compare the latency and complexity of SC-PLDPCH-CC decoder and PLDPCH-BC decoder [20], [40]. We define “latency” as the time interval between (i) the LLR information entering a decoder and (ii) the corresponding decoded P-VNs output from the decoder. We assume a two-step lifting process with the factors z_1 and z_2 applied to lift the base matrices of SC-PLDPCH-CC and PLDPCH-BC. Moreover, layered decoding is used in both cases. For a given PLDPCH-BC, we denote the time taken to complete one decoding iteration by T_r , which has been shown to be proportional to the number of layers, i.e., mz_1 [40]. Denoting the maximum number of iterations by I_{BC} , the time delay (i.e., latency) for decoding one PLDPCH-BC codeword equals $T_{\text{PLDPCH-BC}} = I_{BC}T_r$.

Based on the same protomatrix as the PLDPCH-BC, we use the edge spreading approach to construct an SC-PLDPCH-CC. We exploit the pipeline decoding method in the previous section with I identical processors, each of which applies the layered decoding algorithm. Moreover, it can be readily shown that the design used to implement the aforementioned PLDPCH-BC decoder [40] can be slightly modified to implement these processors. As each processor needs to update mz_1 layers of information whenever a new set of $\{L_{ch}^P(t), L_{ch}^D(t)\}$

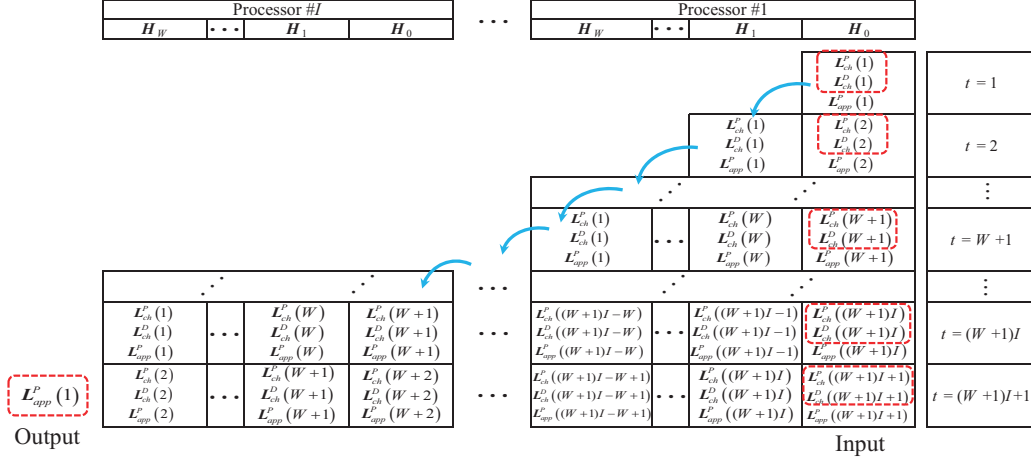


Fig. 3. Structure of a pipeline SC-PLDPCH-CC decoder consisting of I processors (PLDPCH-Hadamard block sub-decoders). $\{\mathbf{L}_{ch}^P(t), \mathbf{L}_{ch}^D(t)\}$ ($t = 1, 2, \dots$) are input into the decoder one set by one set. Every time, all sets of LLRs inside the decoder are shifted to the left, and all APP-LLRs of all P-VNs inside the different I processors are updated. When $\{\mathbf{L}_{ch}^P((W+1)I + t'), \mathbf{L}_{ch}^D((W+1)I + t')\}$ ($t' = 1, 2, \dots$) is input to the decoder, the APP-LLRs $\mathbf{L}_{app}^P(t')$ are output and the values of the coded bits $\mathbf{P}(t')$ are determined.

($t = 1, 2, \dots$) enters the decoder, the time taken is the same as for the PLDPCH-BC decoder to complete one iteration, i.e., T_r . As shown in Fig. 3 and discussed in the previous section, the APP-LLRs $\mathbf{L}_{app}^P(t')$ are output from the decoder when $\{\mathbf{L}_{ch}^P((W+1)I + t'), \mathbf{L}_{ch}^D((W+1)I + t')\}$ is input to the pipeline decoder. Thus, the total time delay (i.e., latency) for decoding one set of input equals $T_{SC-PLDPCH-CC} = (W+1)IT_r$. In addition, $(W+1)I$ sets of LLRs corresponding to different t 's are being processed by the pipeline decoder, as compared to only one set of LLRs being processed by the PLDPCH-BC decoder at any time.

In summary, when a PLDPCH-BC and an SC-PLDPCH-CC are “derived” from the same protomatrix of size $m \times n$ with the same lifting factors z_1 and z_2 , the PLDPCH-BC decoder and each processor in an SC-PLDPCH-CC pipeline decoder processes the mz_1 layers in layered decoding with the same time delay. The SC-PLDPCH-CC pipeline decoder consists of I processors, each having a similar structure as a PLDPCH-BC decoder; and requires $(W+1)I$ times memory storage compared with a PLDPCH-BC decoder. The latencies of the SC-PLDPCH-CC pipeline decoder and PLDPCH-BC decoder are $T_{SC-PLDPCH-CC} = (W+1)IT_r$ and $T_{PLDPCH-BC} = I_{BC}T_r$, respectively. Under the condition that the two latencies are identical, i.e., $T_{SC-PLDPCH-CC} = T_{PLDPCH-BC}$ or $(W+1)I = I_{BC}$, the SC-PLDPCH-CC pipeline decoder achieves a $(W+1)I$ times throughput compared

with the PLDPCH-BC decoder.

3) *SC-PLDPCH-CC and PLDPCH-BC under the same constraint length/blocklength:* In this section, we further compare the case when the constraint length of a SC-PLDPCH-CC is the same as the blocklength of a PLDPCH-BC. We assume a two-step lifting process with the factors z_1 and z_2 applied to lift the $m \times n$ base matrices of SC-PLDPCH-CC and, z'_1 and z'_2 applied to lift the same size base matrix of PLDPCH-BC. The constraint length of the SC-PLDPCH-CC is $L_{CC-CL} = (W+1)N + M(2^r - r - 2) = (W+1)z_1z_2n + z_1z_2m(2^r - r - 2)$ and the blocklength of the PLDPCH-BC is $L_{BC-BL} = z'_1z'_2n + z'_1z'_2m(2^r - r - 2)$. For simplicity, we let $z_1 = z'_1$. When $L_{CC-CL} = L_{BC-BL}$, we have $\delta_{z_2} \triangleq z'_2/z_2 = 1 + \frac{W}{1+(2^r-r-2)\frac{m}{n}}$. The result implies that z'_2 is strictly larger than z_2 . For example, when $W = 1, m = 7, n = 11, r = 4$, we obtain $\delta_{z_2} = z'_2/z_2 = 1.136$. When the number of H-CNs in one layer is increased by a factor of δ_{z_2} , the time taken to complete one decoding iteration is increased by the same factor. In order to maintain the same decoding latency, the maximum number of iterations for decoding one PLDPCH-BC codeword should be reduced by the same factor, i.e., reduced from I_{BC} (see above section) to $I'_{BC} = I_{BC}/\delta_{z_2}$.

²Note that when r is odd, $\delta_{z_2} = 1 + \frac{W}{1+(2^r-2)\frac{m}{n}}$

$$B_0 = \begin{bmatrix} 1 & 0 & 0 & 0 & 0 & 0 & 0 & 0 & 0 & 0 & 1 \\ 0 & 0 & 1 & 0 & 0 & 0 & 0 & 0 & 0 & 1 & 0 \\ 1 & 0 & 0 & 0 & 0 & 0 & 0 & 0 & 0 & 0 & 0 \\ 0 & 0 & 0 & 3 & 0 & 0 & 0 & 0 & 0 & 2 & 0 \\ 0 & 0 & 0 & 0 & 0 & 0 & 0 & 0 & 0 & 0 & 0 \\ 1 & 0 & 0 & 2 & 0 & 0 & 1 & 0 & 0 & 0 & 0 \\ 0 & 0 & 0 & 0 & 0 & 0 & 0 & 0 & 1 & 0 & 0 \end{bmatrix}; \quad B_1 = \begin{bmatrix} 0 & 0 & 0 & 0 & 0 & 0 & 1 & 0 & 3 & 0 & 0 \\ 0 & 1 & 1 & 0 & 0 & 0 & 0 & 0 & 0 & 1 & 1 \\ 1 & 1 & 0 & 0 & 1 & 1 & 0 & 0 & 0 & 0 & 1 \\ 0 & 1 & 0 & 0 & 0 & 0 & 0 & 0 & 0 & 0 & 0 \\ 2 & 0 & 0 & 0 & 0 & 0 & 0 & 1 & 0 & 3 & 0 \\ 2 & 0 & 0 & 0 & 0 & 0 & 0 & 0 & 0 & 0 & 0 \\ 1 & 0 & 0 & 1 & 1 & 0 & 0 & 0 & 0 & 2 & 0 \end{bmatrix} \quad (6)$$

$$B_0 = \begin{bmatrix} 0 & 0 & 0 & 0 & 0 & 0 & 0 & 0 & 0 & 0 & 0 \\ 0 & 1 & 2 & 0 & 0 & 0 & 0 & 0 & 0 & 0 & 0 \\ 2 & 1 & 0 & 0 & 1 & 0 & 0 & 0 & 0 & 0 & 1 \\ 0 & 0 & 0 & 3 & 0 & 0 & 0 & 0 & 0 & 1 & 0 \\ 0 & 0 & 0 & 0 & 0 & 0 & 0 & 1 & 0 & 3 & 0 \\ 2 & 0 & 0 & 1 & 0 & 0 & 0 & 0 & 0 & 0 & 0 \\ 1 & 0 & 0 & 1 & 0 & 0 & 0 & 0 & 0 & 0 & 0 \end{bmatrix}; \quad B_1 = \begin{bmatrix} 1 & 0 & 0 & 0 & 0 & 0 & 1 & 0 & 3 & 0 & 1 \\ 0 & 0 & 0 & 0 & 0 & 0 & 0 & 0 & 0 & 2 & 1 \\ 0 & 0 & 0 & 0 & 0 & 1 & 0 & 0 & 0 & 0 & 0 \\ 0 & 1 & 0 & 0 & 0 & 0 & 0 & 0 & 0 & 1 & 0 \\ 2 & 0 & 0 & 0 & 0 & 0 & 0 & 0 & 0 & 0 & 0 \\ 1 & 0 & 0 & 1 & 0 & 0 & 1 & 0 & 0 & 0 & 0 \\ 0 & 0 & 0 & 0 & 1 & 0 & 0 & 0 & 1 & 2 & 0 \end{bmatrix} \quad (7)$$

D. Layered PEXIT Algorithm

In [16], a low-complexity PEXIT chart technique has been proposed to evaluate the theoretical threshold of PLDPCH-BCs. The thresholds of SC-PLDPCH-CCs are expected to be comparable to those of their underlying block codes. However, direct analysis of SC-PLDPCH-CCs with infinite length is very complicated and time-consuming, which is not conducive to the optimal design of the codes in the next section, i.e., Section IV-E.

As mentioned in Section IV-A, under the same set of split protomatrices $\{B_0, B_1, \dots, B_W\}$, SC-PLDPCH-CCs can be obtained by extending the coupling length L of SC-PLDPCH-TDCs to infinity. An SC-PLDPCH-TDC can be treated as a PLDPCH-BC with a large size and hence its threshold can be evaluated using the original PEXIT chart method in [16]. For SC-PLDPCH-TDCs constructed with different split protomatrices, the original PEXIT chart method will generate different (i.e., distinguishable) thresholds³. For example, Fig. 4 shows the thresholds for two different SC-PLDPCH-TDCs using the original PEXIT chart method. We set $W = 1$. Based on the optimal protomatrix B in [16], the split protomatrices of SC-PLDPCH-TDC #1 are shown as (6) and the split protomatrices of SC-PLDPCH-TDC #2 are shown as (7), where $B_0 + B_1 = B$. From Fig. 4, we can observe that the thresholds of two SC-PLDPCH-TDCs are distinguishable and improved (reduced) as the coupling length L increases. Moreover, the improvement diminishes as L becomes large. Thus, threshold saturation is observed. Subsequently, we

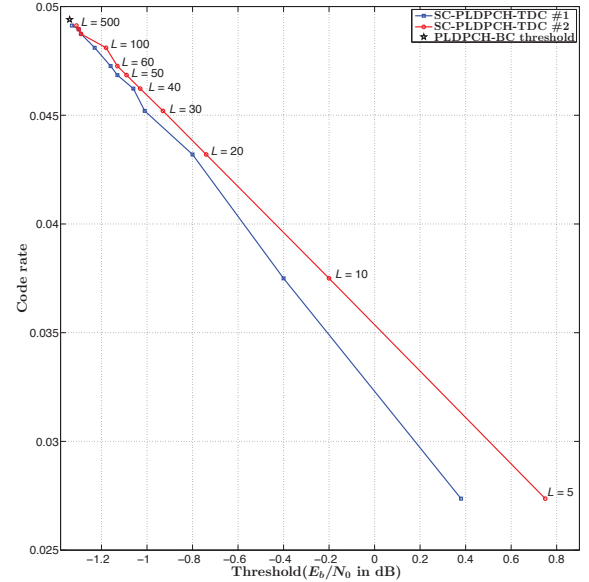


Fig. 4. Distinguishable thresholds for two different SC-PLDPCH-TDCs corresponding to different set of protomatrices $\{B_0, B_1\}$. $W = 1$. Their underlying block code is the optimal $r = 4$ PLDPCH-BC [16] with the decoding threshold indicated by the symbol \star .

select the protomatrices with good thresholds (i.e., low E_b/N_0) to construct the corresponding SC-PLDPCH-CCs.

To improve the convergence rate of the original PEXIT chart method, we propose a layered PEXIT method to analyze the SC-PLDPCH-TDCs. We first define $I_{av}(i, j)$ as the *a priori* mutual information (MI) from the i -th H-CN to the j -th P-VN; $I_{ev}(i, j)$ as the extrinsic MI from the j -th P-VN to the i -th H-CN; $I_{ah}(k)$ as the *a priori* MI of the k -th information bit in the i -th H-CN; $I_{eh}(k)$ as the extrinsic MI of the k -th information bit in the i -

³For SC-PLDPCH-TDCs constructed with different split protomatrices but arrived at the same threshold, we further verify their error performance by simulations.

th H-CN; $I_{app}(j)$ as the *a posteriori* MI of the j -th P-VN; $\sigma_{app}(j)$ as the *a posteriori* information of the j -th P-VN; and $\sigma_{temp}(j)$ as the temporary value of $\sigma_{app}(j)$. We also assume that the channel LLR value L_{ch} follows a normal distribution $\mathcal{N}(\sigma_{L_{ch}}^2/2, \sigma_{L_{ch}}^2)$, where $\sigma_{L_{ch}}^2 = 8R \cdot E_b/N_0$, R is the code rate of SC-PLDPCH-TDC, and E_b/N_0 is the bit-energy-to-noise-power-spectral-density ratio. When the output MI from P-VN or H-CN processors is I_{MI} , we suppose that the corresponding LLR values of the extrinsic information obey a normal distribution $\mathcal{N}(\pm\sigma^2/2, \sigma^2)$. The relationship between I_{MI} and σ can be approximately computed by the functions $I_{MI} = J(\sigma)$ and $\sigma = J^{-1}(I_{MI})$ in [41], [42].

Given a coupling width W and a set of protomatrices $\{\mathbf{B}_0, \mathbf{B}_1, \dots, \mathbf{B}_W\}$ each of size $m \times n$, we use these protomatrices to construct an SC-PLDPCH-TDC with the coupling width W and an appropriate coupling length L . The protomatrix of the SC-PLDPCH-TDC $\mathbf{B}_{SC-PLDPCH-TDC} = \{b_{TDC}(i, j)\}$ therefore has a size of $m(L + W) \times nL$. In (8), the protomatrix \mathbf{B} of size $m \times n = 3 \times 4$ is split into \mathbf{B}_0 and \mathbf{B}_1 of the same size assuming $W = 1$. Based on \mathbf{B}_0 and \mathbf{B}_1 , an SC-PLDPCH-TDC with $W = 1$ and $L = 2$ is constructed in (9) and has a size of $m(L + W) \times nL = 9 \times 8$. Note that in computing the threshold of the SC-PLDPCH-TDC, a larger L , e.g., $L = 10$, will be used for threshold evaluation such that $nL > m(L + W)$.

Similar to the decoding strategy in the layered decoder [20], the layered PEXIT method proceeds as follows.

- 1) Set the initial E_b/N_0 in dB (i.e., $E_b/N_0(\text{dB})$)⁴.
- 2) Set the maximum number of iterations $N_{\max} = 150$.
- 3) Compute $\sigma_{L_{ch}} = (8R \cdot 10^{(E_b/N_0(\text{dB}))/10})^{1/2}$ for L_{ch} , and set $\sigma_{app}(j) = \sigma_{L_{ch}}$ for $j = 1, 2, \dots, nL$.
- 4) For $i = 1, 2, \dots, m(L + W)$ and $j = 1, 2, \dots, nL$, set $I_{av}(i, j) = 0$.
- 5) Set the iteration number $N_{it} = 1$.
- 6) Set $i = 1$.
- 7) For $j = 1, 2, \dots, nL$, subtract $b_{TDC}(i, j) \times (J^{-1}(I_{av}(i, j)))^2$ from $(\sigma_{app}(j))^2$, and then

compute $\sigma_{temp}(j)$ using (10).

- 8) For $j = 1, 2, \dots, nL$, compute (11) if $b_{TDC}(i, j) > 0$; otherwise set $I_{ev}(i, j) = 0$.

Taking the first row of the 9×8 protomatrix $\mathbf{B}_{SC-PLDPCH-TDC}$ in (9) as an example, we obtain the 1×8 vector $\mathbf{b}_{TDC}(1, :)$ shown in (12). After analyzing the MI of the P-VNs, the corresponding 1×8 MI vector $\mathbf{I}_{ev}(1, :)$ is shown in (13).

- 9) Convert the $1 \times nL$ $\mathbf{I}_{ev}(i, :)$ MI vector into a $1 \times d$ \mathbf{I}_{ah} MI vector by eliminating the 0 entries and repeating $b_{TDC}(i, j) (\geq 1)$ times the entry $I_{ev}(i, j)$.

Remark: Each row weight of a protomatrix \mathbf{B} for the underlying PLDPCH-BC equals $d = r + 2$ [16] and hence each row corresponds to a $r = d - 2$ Hadamard code. However, due to the structure of SC-PLDPCH-TDCs, the first and last Wm rows in $\mathbf{B}_{SC-PLDPCH-TDC}$ contain only part of the structure $[\mathbf{B}_W \dots \mathbf{B}_1 \mathbf{B}_0]$ ($\mathbf{B} = \sum_{i=0}^W \mathbf{B}_i$) and thus the row weight could be less than d . For simplicity and uniformity, we compute the MI values of $r = d - 2$ Hadamard code for each row (i.e., each H-CN). For the first/last Wm rows in $\mathbf{B}_{SC-PLDPCH-TDC}$, when their row weight d_1 is less than d , the first/last $d - d_1$ MI values in \mathbf{I}_{ah} are set to 1⁵. For example, the row weight of the underlying protomatrix \mathbf{B} (8) equals $d = 6$ while the row weight of the 1×8 $\mathbf{b}_{TDC}(1, :)$ equals $d_1 = 3 < d$. Hence, when converting 1×8 $\mathbf{I}_{ev}(1, :)$ into the 1×6 \mathbf{I}_{ah} MI vector, the first $d - d_1 = 3$ values, i.e., $[I_{ah}(1) I_{ah}(2) I_{ah}(3)]$ are set to 1, as shown in (14).

- 10) Based on $\sigma_{L_{ch}}$ and the d entries in \mathbf{I}_{ah} , we use the Monte Carlo method in [16] to generate d extrinsic MI values, i.e., a $1 \times d$ MI vector \mathbf{I}_{eh} ⁶. (For more details of the method, please refer to the Appendices in [16].) We use the same symbol definitions as in [16]. Hence $p_e(\xi|X = x)$ in (15) denotes the PDF of the LLR values given the bit x being “0” or “1”; in (16), $\mathbf{U} = \{U(\alpha, k)\}$ denotes a $w \times d$ matrix in which each row represents a length- d

⁴The initial values will be different according to different codes (corresponding to different Hadamard order r). In our optimization design, given $W = 1$ and $L = 10$, initial E_b/N_0 is -0.30 dB for $r = 4$, -0.40 dB for $r = 5$, -0.80 dB for $r = 8$ and -0.85 dB for $r = 10$, respectively.

⁵MI value equal to 1 means that the corresponding MI is known and does not provide any new information in the analysis.

⁶When MI value equals 1, Monte Carlo method will generate the corresponding LLR values with large absolute values. In our analysis, we set them as ± 100 .

$$\mathbf{B} = \begin{bmatrix} 2 & 0 & 2 & 2 \\ 0 & 2 & 2 & 2 \\ 3 & 2 & 0 & 1 \end{bmatrix}, \mathbf{B}_0 = \begin{bmatrix} 1 & 0 & 0 & 2 \\ 0 & 1 & 1 & 1 \\ 1 & 2 & 0 & 1 \end{bmatrix}, \mathbf{B}_1 = \begin{bmatrix} 1 & 0 & 2 & 0 \\ 0 & 1 & 1 & 1 \\ 2 & 0 & 0 & 0 \end{bmatrix} \quad (8)$$

$$\mathbf{B}_{\text{SC-PLDPCH-TDC}} = \begin{bmatrix} \mathbf{B}_0 & \mathbf{0} \\ \mathbf{B}_1 & \mathbf{B}_0 \\ \mathbf{0} & \mathbf{B}_1 \end{bmatrix} = \begin{bmatrix} 1 & 0 & 0 & 2 & 0 & 0 & 0 & 0 \\ 0 & 1 & 1 & 1 & 0 & 0 & 0 & 0 \\ 1 & 2 & 0 & 1 & 0 & 0 & 0 & 0 \\ 1 & 0 & 2 & 0 & 1 & 0 & 0 & 2 \\ 0 & 1 & 1 & 1 & 0 & 1 & 1 & 1 \\ 2 & 0 & 0 & 0 & 1 & 2 & 0 & 1 \\ 0 & 0 & 0 & 0 & 1 & 0 & 2 & 0 \\ 0 & 0 & 0 & 0 & 0 & 1 & 1 & 1 \\ 0 & 0 & 0 & 0 & 2 & 0 & 0 & 0 \end{bmatrix} \quad (9)$$

$$\sigma_{\text{temp}}(j) = \sqrt{(\sigma_{\text{app}}(j))^2 - b_{\text{TDC}}(i, j) \times (J^{-1}(I_{\text{av}}(i, j)))^2} \quad \forall j \quad (10)$$

$$I_{\text{ev}}(i, j) = J \left(\sqrt{(\sigma_{\text{app}}(j))^2 - (J^{-1}(I_{\text{av}}(i, j)))^2} \right) \quad \forall j \quad (11)$$

$$\mathbf{b}_{\text{TDC}}(1, :) = [1 \ 0 \ 0 \ 2 \ 0 \ 0 \ 0 \ 0] \quad (12)$$

$$\mathbf{I}_{\text{ev}}(1, :) = [I_{\text{ev}}(1, 1) \ 0 \ 0 \ I_{\text{ev}}(1, 4) \ 0 \ 0 \ 0 \ 0] \quad (13)$$

$$\begin{aligned} \mathbf{I}_{\text{ah}} &= [I_{\text{ah}}(1) \ I_{\text{ah}}(2) \ I_{\text{ah}}(3) \ I_{\text{ah}}(4) \ I_{\text{ah}}(5) \ I_{\text{ah}}(6)] \\ &= [1 \ 1 \ 1 \ I_{\text{ev}}(1, 1) \ I_{\text{ev}}(1, 4) \ I_{\text{ev}}(1, 4)] \end{aligned} \quad (14)$$

$$I_{\text{eh}}(k) = \frac{1}{2} \sum_{x \in \{0,1\}} \int_{-\infty}^{\infty} p_e(\xi|X=x) \log_2 \frac{2 \cdot p_e(\xi|X=x)}{p_e(\xi|X="0") + p_e(\xi|X="1")} d\xi \quad (15)$$

$$\approx 1 - \frac{1}{w} \sum_{\alpha=1}^w \log_2 \left(1 + e^{-(1-2U(\alpha, k)) \times V(\alpha, k)} \right) \quad (16)$$

$$\mathbf{I}_{\text{eh}} = [I_{\text{eh}}(1) \ I_{\text{eh}}(2) \ I_{\text{eh}}(3) \ I_{\text{eh}}(4) \ I_{\text{eh}}(5) \ I_{\text{eh}}(6)] \quad (17)$$

$$\begin{aligned} \mathbf{I}_{\text{av}}(1, :) &= [I_{\text{av}}(1, 1) \ 0 \ I_{\text{av}}(1, 3) \ 0 \ 0 \ 0 \ 0 \ 0] \\ &= \left[I_{\text{eh}}(4) \ 0 \ \frac{1}{2} \sum_{k=5}^6 I_{\text{eh}}(k) \ 0 \ 0 \ 0 \ 0 \ 0 \right] \end{aligned} \quad (18)$$

$$\sigma_{\text{app}}(j) = \sqrt{(\sigma_{\text{temp}}(j))^2 + b_{\text{TDC}}(i, j) \times (J^{-1}(I_{\text{av}}(i, j)))^2} \quad \forall j \quad (19)$$

SPC codeword and $\mathbf{V} = \{V(\alpha, k)\}$ denotes a $w \times d$ matrix in which each row represents a set of (d) extrinsic LLR values generated by the Hadamard decoder.

Using the previous example, the MI vector \mathbf{I}_{eh} is shown in (17).

- 11) Convert the $1 \times d$ \mathbf{I}_{eh} MI vector into a $1 \times nL$ $\mathbf{I}_{\text{av}}(i, :)$ MI vector. For $j = 1, 2, \dots, nL$, if $b_{\text{TDC}}(i, j) > 0$, set the value of $I_{\text{av}}(i, j)$ as the average of the corresponding $b_{\text{TDC}}(i, j)$ MI values in \mathbf{I}_{eh} ; otherwise set $I_{\text{av}}(i, j) = 0$. For the first/last Wm rows in $\mathbf{B}_{\text{SC-PLDPCH-TDC}}$, when their row weight d_1 is less than d , the first/last $d-d_1$ MI values in \mathbf{I}_{eh} will be omitted, and the remaining d_1 values will be used to compute $\mathbf{I}_{\text{av}}(i, :)$.

In the above example, we omit the first $d-d_1 =$

3 MI values in \mathbf{I}_{eh} , i.e., $[I_{\text{eh}}(1) \ I_{\text{eh}}(2) \ I_{\text{eh}}(3)]$, and use the remaining $d_1 = 3$ MI values, i.e., $[I_{\text{eh}}(4) \ I_{\text{eh}}(5) \ I_{\text{eh}}(6)]$ to compute the $\mathbf{I}_{\text{av}}(1, :)$ MI vector given in (18).

- 12) For $j = 1, 2, \dots, nL$, use the “new” extrinsic information $\mathbf{I}_{\text{av}}(i, :)$ to update the *a posteriori* information $\sigma_{\text{app}}(j)$ by (19).
- 13) If i is smaller than the number of rows ($m(L+W)$), increment i by 1 and go to Step 7).
- 14) For $j = 1, 2, \dots, nL$, compute $I_{\text{app}}(j) = J(\sigma_{\text{app}}(j))$. If $I_{\text{app}}(j) = 1 \ \forall j$, decrement E_b/N_0 by 0.05 dB and go to Step 3);
- 15) If the maximum number of iterations is not reached, increment N_{it} by 1 and go to Step 6); otherwise, stop and the threshold is given by $(E_b/N_0)^* = E_b/N_0 + 0.05 \text{ dB}$.

As can be observed, the proposed layered PEXIT

TABLE I

NUMBER OF ITERATIONS N_{it} REQUIRED FOR THE PEXIT ALGORITHMS TO CONVERGE AT DIFFERENT E_b/N_0 . THE MAXIMUM NUMBER OF ITERATIONS IS $N_{\max} = 150$ FOR THE LAYERED PEXIT CHART ALGORITHM AND $2N_{\max} = 300$ FOR THE ORIGINAL PEXIT CHART ALGORITHM.

E_b/N_0 in dB	-0.30	-0.35	-0.40
Original PEXIT [16]	107	190	197
Proposed layered PEXIT	80	104	121

chart algorithm updates the corresponding *a posteriori* information (using Step 12)) every time the extrinsic MI of one row (layer) is obtained. Further, we set $L = 10$ and construct an SC-PLDPCH-TDC with a protomatrix $\mathbf{B}_{\text{SC-PLDPCH-TDC}}$ of size 77×110 (where \mathbf{B}_0 and \mathbf{B}_1 are given by (6)). Table I lists the number of iterations required for the original PEXIT algorithm [16] and our proposed layered PEXIT algorithm to converge as E_b/N_0 changes from -0.30 dB to -0.40 dB. We observe that our layered PEXIT algorithm reduces the number of iterations by at least 30% compared with the original PEXIT algorithm. The number of iterations is reduced by 62.8% at $E_b/N_0 = -0.40$ dB. We also find that both algorithms do not converge at $E_b/N_0 = -0.45$ dB when the maximum number of iterations is set to $N_{\max} = 150$ for the layered PEXIT chart method, and is set to $2N_{\max} = 300$ for original PEXIT chart method. Thus both algorithms arrive at the same decoding threshold, i.e., $(E_b/N_0)^* = -0.40$ dB. The proposed layered PEXIT algorithm can therefore speed up the convergence rate when calculating the threshold of SC-PLDPCH-TDCs.

Remark: The difference between our proposed layered PEXIT algorithm and the shuffled EXIT algorithm [43] are as follows.

- Given a protomatrix, our algorithm performs the analysis row by row, while the shuffled EXIT algorithm [43] performs the analysis column by column.
- When analyzing SC-PLDPCH-TDCs, our algorithm computes MI values for Hadamard check nodes, while [43] computes MI values for SPC-CN.

E. Optimizing Protomatrices using Genetic Algorithm

To solve a problem based on GA [44], a generation group is first created or initialized and a fitness function is developed to calculate the fitness value of each individual in the group. Based on the fitness values, some individuals are selected from the “parent” generation group to form an “offspring” generation group. To facilitate obtaining good solutions, the individuals having the best fitness values in the parent generation group will be kept in the offspring generation group. Crossover and mutation operations are further performed in the offspring generation group. Subsequently, the “offspring” generation group becomes the “parent” generation group. By repeating the generation cycles, GA has a high probability of arriving at the global optimal solution to the problem [28]. Given a protomatrix \mathbf{B} corresponding to a PLDPCH-BC, we propose a GA to systematically search for optimized sets of protomatrices $\{\mathbf{B}_0, \mathbf{B}_1, \dots, \mathbf{B}_W\}$ (where $\mathbf{B} = \sum_{i=0}^W \mathbf{B}_i$) for the corresponding SC-PLDPCH-TDC. By selecting SC-PLDPCH-TDCs with good thresholds, our final objective is to design optimal SC-PLDPCH-CCs based on the same set of protomatrices. We denote

- K parent individuals Φ^k ($k = 1, 2, \dots, K$) as K sets of $W + 1$ protomatrices, i.e., $\Phi^k = \{\mathbf{B}_0^k, \mathbf{B}_1^k, \dots, \mathbf{B}_W^k\}$, each of which satisfies $\mathbf{B} = \sum_{i=0}^W \mathbf{B}_i^k$;
- the fitness function as $\psi(\cdot)$ and the fitness value of the k -th parent individual as $f_k = \psi(\Phi^k)$;
- the probability of selecting the k -th parent individual as p_{s_k} ;
- the probability of crossover as p_c and the probability of mutation as p_m ;
- K offspring individuals Υ_k ($k = 1, 2, \dots, K$) as K sets of $W + 1$ protomatrices, i.e., $\Upsilon_k = \{\mathbf{S}_0^k, \mathbf{S}_1^k, \dots, \mathbf{S}_W^k\}$, each of which satisfies $\mathbf{B} = \sum_{i=0}^W \mathbf{S}_i^k$;
- $m \times n$ as the size of \mathbf{B} , and hence also the size of \mathbf{B}_i^k and \mathbf{S}_i^k for all i and k ;
- N_g as the number of individuals having good fitness values.

Our proposed GA algorithm is described as follows.

- 1) Initialization: Set coupling width W , coupling length L , and the number of individuals K in each generation. Randomly generate K sets of $\Phi^k = \{\mathbf{B}_0^k, \mathbf{B}_1^k, \dots, \mathbf{B}_W^k\}$, $k = 1, 2, \dots, K$.

- 2) Computation of fitness values: For each Φ^k , we construct the corresponding SC-PLDPCH-TDC by coupling L sets of Φ^k . Then we apply our proposed layered PEXIT chart method in Section IV-D to analyze the threshold and convergence behavior of the SC-PLDPCH-TDC. Recall that for a specific E_b/N_0 value (in dB), the iteration number required to converge is given by N_{it} and the maximum number of iterations is given by N_{max} . Our proposed fitness function $\psi(\cdot)$ takes both the number of successful convergences, denoted by N_c , and the convergence rate N_{it} into consideration. We define $\psi(\cdot)$ as

$$\psi(\Phi^k) = f_k = \sum_{i=1}^{N_c} [N_{max} - N_{it,i}^k] = N_c N_{max} - \sum_{i=1}^{N_c} N_{it,i}^k \quad (20)$$

where $N_{it,i}^k$ represents the number of iterations for the SC-PLDPCH-TDC corresponding to Φ^k to converge in the i -th successful convergence ($i = 1, 2, \dots, N_c$). Note that $\psi(\Phi^k)$ should give a larger value if the corresponding SC-PLDPCH-TDC converges faster and more times in the layered PEXIT algorithm.

In the example given in Table I, the layered PEXIT algorithm has converged at -0.30 dB, -0.35 dB and -0.40 dB, and hence $N_c = 3$. Using (20), the fitness value of $\{\mathbf{B}_0, \mathbf{B}_1\}$ defined in (6) is therefore given by $\psi(\{\mathbf{B}_0, \mathbf{B}_1\}) = 3 \times 150 - (80 + 104 + 121) = 145$.

- 3) Selection: Compute the fitness values $f_k = \psi(\Phi^k)$ for the K parent individuals Φ^k ($k = 1, 2, \dots, K$). Subsequently, we normalize f_k ($k = 1, 2, \dots, K$) to form the probabilities of selection, i.e., $p_{s_k} = f_k / \sum_{j=1}^K f_j$; $k = 1, 2, \dots, K$. Then the K offspring individuals $\Upsilon_{k'}$ ($k' = 1, 2, \dots, K$) are chosen from the parent generation group Φ^k ($k = 1, 2, \dots, K$) as follows. First, the N_g individuals with the highest fitness values in the parent group are passed to the offspring group directly to fill $\Upsilon_{k'}$ ($k' = 1, 2, \dots, N_g$). Then to fill each of the remaining $K - N_g$ offspring slots, i.e., $\Upsilon_{k'}$ ($k' = N_g + 1, N_g + 2, \dots, K$), a random parent individual Φ^k is selected accordingly to the probability p_{s_k} . These $K - N_g$ offsprings will further go through the crossover and mutation processes below.
- 4) Crossover: Assuming $K - N_g$ is even, the

$K - N_g$ selected offspring individuals, i.e., $\Upsilon_{k'}$ ($k' = N_g + 1, N_g + 2, \dots, K$) are randomly divided into $(K - N_g)/2$ pairs. For each pair $\Upsilon_{k_1} = \{\mathbf{S}_0^{k_1}, \mathbf{S}_1^{k_1}, \dots, \mathbf{S}_W^{k_1}\}$ and $\Upsilon_{k_2} = \{\mathbf{S}_0^{k_2}, \mathbf{S}_1^{k_2}, \dots, \mathbf{S}_W^{k_2}\}$, we select two random positions (u_1, v_1) and (u_2, v_2) where $1 \leq u_1 \leq u_2 \leq m$ and $1 \leq v_1 \leq v_2 \leq n$. With a probability of p_c , all entries between (u_1, v_1) and (u_2, v_2) (in a column-wise manner) in $\mathbf{S}_i^{k_1}$ are exchanged with the corresponding entries in $\mathbf{S}_i^{k_2}$ ($i = 0, 1, \dots, W$).

Fig. 5(a) shows a crossover example where $m \times n = 3 \times 4$. The pair of offspring individuals selected are given by $\Upsilon_{k_1} = \{\mathbf{S}_0^{k_1}, \mathbf{S}_1^{k_1}\}$ and $\Upsilon_{k_2} = \{\mathbf{S}_0^{k_2}, \mathbf{S}_1^{k_2}\}$ ($N_g < k_1 \neq k_2 \leq K$). The two selected positions are $(u_1, v_1) = (2, 2)$ and $(u_2, v_2) = (2, 3)$. Hence the entries in positions $(2, 2), (3, 2), (1, 3), (2, 3)$ are exchanged between $\mathbf{S}_0^{k_1}$ and $\mathbf{S}_0^{k_2}$; and are exchanged between $\mathbf{S}_1^{k_1}$ and $\mathbf{S}_1^{k_2}$.

- 5) Mutation: The offspring individuals $\Upsilon_{k'} = \{\mathbf{S}_0^{k'}, \mathbf{S}_1^{k'}, \dots, \mathbf{S}_W^{k'}\}$ that have gone through the crossover process will then be considered for mutation separately. Within each offspring individual, one random position (u, v) ($1 \leq u \leq m$ and $1 \leq v \leq n$) corresponding to a non-zero entry in \mathbf{B} are selected. For all the (u, v) -th entries in $\mathbf{S}_0^{k'}, \mathbf{S}_1^{k'}, \dots, \mathbf{S}_W^{k'}$, they are mutated together with a probability of p_m . The entries should have different values after the mutation while keeping $\sum_{i=0}^W \mathbf{S}_i^{k'} = \mathbf{B}$ satisfied.

Fig. 5(b) illustrates a mutation example. The offspring individual being considered is $\Upsilon_{k_1} = \{\mathbf{S}_0^{k_1}, \mathbf{S}_1^{k_1}\}$ ($N_g < k_1 \leq K$) and mutation occurs in all the $(3, 1)$ -th entries, where the $(3, 1)$ -th entry in $\mathbf{B} = \mathbf{S}_0^{k_1} + \mathbf{S}_1^{k_1}$ (8) equals 3 and hence is non-zero.

- 6) Set $\Phi_k = \Upsilon_k$, $k = 1, 2, \dots, K$.
- 7) Repeat Steps 2) to 6) until $\exists \Phi_k$ such that the corresponding SC-PLDPCH-TDC has a low threshold and the derived SC-PLDPCH-CC has a good error performance at low E_b/N_0 .

When GA is used to systematically search for good protomatrices, setting $L = 10$ in the layered PEXIT algorithm can efficiently calculate the threshold of an SC-PLDPCH-TDC. Once good protomatrices are found, we increase L so that the code rate of the SC-PLDPCH-TDC is very close

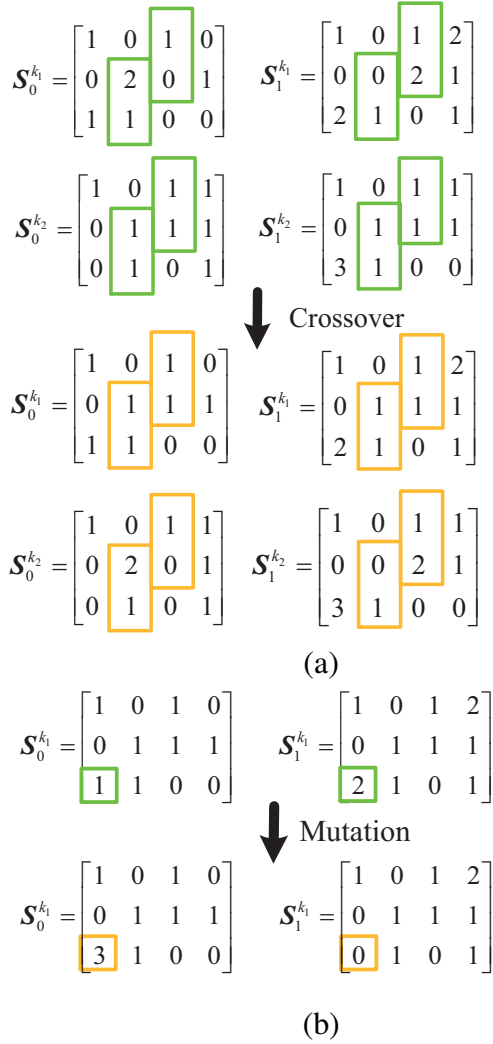


Fig. 5. (a) Crossover example. The pair of offspring individuals are $\Upsilon_{k_1} = \{S_0^{k_1}, S_1^{k_1}\}$ and $\Upsilon_{k_2} = \{S_0^{k_2}, S_1^{k_2}\}$ ($N_g < k_1 \neq k_2 \leq K$). Two selected positions are $(u_1, v_1) = (2, 2)$ and $(u_2, v_2) = (2, 3)$. The entries in positions $(2, 2), (3, 2), (1, 3), (2, 3)$ of $S_0^{k_1}$, i.e., $[2 \ 1 \ 1 \ 0]$ are exchanged with those in the same positions of $S_0^{k_2}$, i.e., $[1 \ 1 \ 1 \ 1]$. Similarly, $[0 \ 1 \ 1 \ 2]$ in $S_1^{k_1}$ are exchanged with $[1 \ 1 \ 1 \ 1]$ in $S_1^{k_2}$. (b) Mutation example. $\Upsilon_1 = \{S_0^{k_1}, S_1^{k_1}\}$ ($N_g < k_1 \leq K$) and mutation occurs in all the $(3, 1)$ -th entries. The entry 1 in $S_0^{k_1}$ is changed into 3 and the entry 2 in $S_1^{k_1}$ is changed into 0 to keep $S_0^{k_1} + S_1^{k_1} = B$ (8).

to that of its SC-PLDPCH-CC. We then use the layered PEXIT method to calculate the threshold of the lengthened SC-PLDPCH-TDC as proxy for the SC-PLDPCH-CC threshold.

V. SIMULATION RESULTS

Based on the optimized PLDPCH-BCs found in [16], we search for good SC-PLDPCH-CCs using the layered PEXIT algorithm and the GA proposed in Section IV-D and Section IV-E. We assume $W = 1$, and use $L = 10$ and $N_{\max} = 150$ in

TABLE II
THRESHOLDS FOR SC-PLDPCH-TDCs AND PLDPCH-BCs [16]
COMPUTED BY THE PROPOSED PEXIT ALGORITHM.
 $N'_{\max} = 1000$. FOR SC-PLDPCH-TDCs, COUPLING WIDTH
 $W = 1$ AND COUPLING LENGTH $L = 500$ FOR $r = 4$; $L = 300$
FOR $r = 5, 8$; AND $L = 100$ FOR $r = 10$.

Code		TDC	BC [16]
$r = 4$	Code rate R	0.0491	0.0494
	Threshold in dB	-1.35	-1.34
$r = 5$	Code rate R	0.021	0.021
	Threshold in dB	-1.37	-1.37
$r = 8$	Code rate R	0.008	0.008
	Threshold in dB	-1.45	-1.44
$r = 10$	Code rate R	0.00291	0.00295
	Threshold in dB	-1.48	-1.50

the layered PEXIT method. We also set $K = 30$, $N_g = 4$, $p_c = 0.8$ and $p_m = 0.6$ in the GA. We use binary phase-shift-keying (BPSK) modulation over an AWGN channel. Moreover, we apply the pipeline decoding with different number of processors to evaluate the error performance of the SC-PLDPCH-CCs found.

For each E_b/N_0 value, simulations are performed for at least 1000 sub-blocks with at least 100 sub-block errors. Then the corresponding BER is evaluated. Under comparable information lengths and code rates, we compare the BER performance of our proposed codes not only with that of the underlying PLDPCH-BC, but also with those of state-of-the-art codes, namely LDPC-Hadamard block code (LDPC-BC) [14], turbo-Hadamard code (THC) [9], irregular zigzag-Hadamard code (IRZHC) [45], [46] (whenever BER results are available). These long codes with good error performance under very low E_b/N_0 values can potentially be applied to deep space communications where the signal from the space probe to Earth is extremely weak; and to embed/transmit hidden information over an ordinary wireless communication link. For $r = 4$ and $r = 5$, we also compare the BER performance of PLDPCH-BCs and SC-PLDPCH-CCs under the same blocklength/constraint length.

A. Rate-0.0494 and $r = 4$

Based on the 7×11 protomatrix B of the optimized rate-0.0494 PLDPCH-BC [16], we apply GA and find two 7×11 protomatrices shown as (21) after 13 generations. The corresponding fitness value equals 554. Then we increase L to

$$B_0 = \begin{bmatrix} 1 & 0 & 0 & 0 & 0 & 0 & 1 & 0 & 1 & 0 & 0 \\ 0 & 0 & 1 & 0 & 0 & 0 & 0 & 0 & 0 & 2 & 1 \\ 2 & 1 & 0 & 0 & 0 & 0 & 0 & 0 & 0 & 0 & 1 \\ 0 & 1 & 0 & 1 & 0 & 0 & 0 & 0 & 0 & 2 & 0 \\ 1 & 0 & 0 & 0 & 0 & 0 & 0 & 1 & 0 & 1 & 0 \\ 1 & 0 & 0 & 2 & 0 & 0 & 0 & 0 & 0 & 0 & 0 \\ 1 & 0 & 0 & 0 & 1 & 0 & 0 & 0 & 0 & 2 & 0 \end{bmatrix} \quad B_1 = \begin{bmatrix} 0 & 0 & 0 & 0 & 0 & 0 & 0 & 0 & 2 & 0 & 1 \\ 0 & 1 & 1 & 0 & 0 & 0 & 0 & 0 & 0 & 0 & 0 \\ 0 & 0 & 0 & 0 & 1 & 1 & 0 & 0 & 0 & 0 & 0 \\ 0 & 0 & 0 & 2 & 0 & 0 & 0 & 0 & 0 & 0 & 0 \\ 1 & 0 & 0 & 0 & 0 & 0 & 0 & 0 & 0 & 2 & 0 \\ 2 & 0 & 0 & 0 & 0 & 0 & 1 & 0 & 0 & 0 & 0 \\ 0 & 0 & 0 & 1 & 0 & 0 & 0 & 0 & 1 & 0 & 0 \end{bmatrix} \quad (21)$$

$$B_0 = \begin{bmatrix} 1 & 2 & 0 & 0 & 0 & 0 & 0 & 0 & 1 & 0 \\ 0 & 0 & 1 & 0 & 0 & 1 & 0 & 2 & 0 & 0 \\ 0 & 0 & 0 & 1 & 1 & 0 & 0 & 0 & 0 & 1 \\ 0 & 0 & 0 & 1 & 0 & 0 & 0 & 2 & 0 & 1 \\ 0 & 0 & 0 & 1 & 0 & 0 & 1 & 2 & 0 & 0 \\ 1 & 0 & 0 & 0 & 0 & 0 & 0 & 1 & 0 & 1 \end{bmatrix} \quad B_1 = \begin{bmatrix} 2 & 0 & 0 & 0 & 1 & 0 & 0 & 0 & 0 & 0 \\ 0 & 0 & 1 & 0 & 0 & 1 & 1 & 0 & 0 & 0 \\ 0 & 0 & 0 & 2 & 0 & 0 & 0 & 1 & 0 & 1 \\ 0 & 1 & 0 & 0 & 0 & 0 & 0 & 0 & 0 & 2 \\ 0 & 0 & 0 & 1 & 0 & 0 & 0 & 0 & 0 & 2 \\ 1 & 0 & 1 & 1 & 0 & 0 & 0 & 1 & 0 & 0 \end{bmatrix} \quad (22)$$

$$B_0 = \begin{bmatrix} 1 & 0 & 1 & 0 & 0 & 0 & 0 & 1 & 0 & 0 & 0 & 1 & 0 & 0 & 0 \\ 0 & 1 & 0 & 0 & 1 & 0 & 0 & 0 & 0 & 0 & 0 & 0 & 2 & 0 & 0 \\ 0 & 0 & 0 & 0 & 0 & 0 & 1 & 0 & 0 & 1 & 1 & 2 & 1 & 0 & 0 \\ 0 & 0 & 0 & 1 & 2 & 0 & 0 & 0 & 0 & 0 & 0 & 3 & 0 & 0 & 1 \\ 0 & 0 & 0 & 0 & 0 & 1 & 0 & 0 & 1 & 1 & 0 & 0 & 1 & 0 & 0 \end{bmatrix} \quad (23)$$

$$B_1 = \begin{bmatrix} 1 & 0 & 0 & 0 & 0 & 0 & 0 & 2 & 2 & 0 & 0 & 0 & 0 & 0 & 1 \\ 0 & 1 & 0 & 1 & 0 & 0 & 0 & 0 & 0 & 0 & 3 & 0 & 1 & 0 & 0 \\ 0 & 0 & 1 & 0 & 0 & 2 & 1 & 0 & 0 & 0 & 0 & 0 & 0 & 0 & 0 \\ 0 & 0 & 0 & 1 & 0 & 0 & 0 & 0 & 0 & 1 & 0 & 0 & 0 & 0 & 1 \\ 0 & 0 & 0 & 0 & 0 & 0 & 1 & 0 & 0 & 0 & 1 & 2 & 2 & 0 & 0 \end{bmatrix}. \quad (24)$$

$$B_0 = \begin{bmatrix} 1 & 0 & 0 & 0 & 0 & 0 & 2 & 0 & 0 & 0 & 0 & 0 & 0 & 0 & 1 & 0 & 0 & 0 & 0 & 1 & 3 & 0 & 1 & 0 \\ 0 & 0 & 0 & 1 & 1 & 0 & 0 & 0 & 1 & 1 & 0 & 0 & 1 & 0 & 0 & 0 & 2 & 0 & 0 & 0 & 0 & 0 & 0 & 0 \\ 0 & 1 & 1 & 0 & 0 & 1 & 0 & 0 & 0 & 0 & 0 & 0 & 0 & 0 & 0 & 0 & 0 & 2 & 0 & 0 & 0 & 0 & 0 \\ 0 & 0 & 0 & 0 & 0 & 0 & 0 & 1 & 0 & 0 & 1 & 1 & 0 & 0 & 0 & 0 & 0 & 0 & 0 & 1 & 1 & 0 & 0 \\ 0 & 1 & 0 & 0 & 0 & 0 & 0 & 0 & 0 & 0 & 0 & 0 & 0 & 0 & 1 & 0 & 1 & 0 & 2 & 0 & 0 & 1 & 0 \\ 0 & 0 & 0 & 0 & 0 & 0 & 0 & 2 & 2 & 2 & 0 & 0 & 0 & 1 & 0 & 0 & 0 & 0 & 0 & 0 & 0 & 0 & 0 \end{bmatrix} \quad (25)$$

$$B_1 = \begin{bmatrix} 0 & 0 & 0 & 0 & 0 & 0 & 1 & 0 & 0 & 0 & 0 & 0 & 0 & 0 & 1 & 0 & 0 & 0 & 0 & 1 & 0 & 0 & 0 \\ 0 & 0 & 0 & 2 & 1 & 0 & 0 & 0 & 0 & 0 & 0 & 0 & 0 & 0 & 1 & 1 & 0 & 0 & 0 & 0 & 0 & 0 & 0 \\ 0 & 0 & 1 & 0 & 0 & 0 & 0 & 0 & 0 & 0 & 0 & 0 & 0 & 0 & 1 & 0 & 0 & 1 & 0 & 4 & 0 & 0 & 0 \\ 0 & 0 & 0 & 0 & 0 & 0 & 0 & 0 & 0 & 2 & 2 & 0 & 0 & 0 & 0 & 0 & 0 & 0 & 0 & 1 & 1 & 0 & 1 \\ 2 & 1 & 0 & 0 & 0 & 0 & 0 & 0 & 0 & 0 & 0 & 0 & 1 & 0 & 0 & 0 & 0 & 0 & 1 & 0 & 0 & 0 & 1 \\ 0 & 0 & 0 & 0 & 0 & 1 & 0 & 1 & 1 & 0 & 0 & 0 & 1 & 0 & 0 & 0 & 0 & 0 & 0 & 1 & 0 & 0 & 0 \end{bmatrix} \quad (26)$$

500 and the code rate of the SC-PLDPCH-TDC constructed by (21) is increased to about 0.0491, approaching that of underlying PLDPCH-BC [16]. Using the proposed layered PEXIT method with $N'_{max} = 1000$ iterations, Table II lists the thresholds for the $r = 4$ SC-PLDPCH-TDC with $L = 500$, and the $r = 4$ PLDPCH-BC⁷ [16], respectively. The theoretical threshold of the terminated code with $L = 500$ is found to be -1.35 dB, which is approximated as the threshold of the SC-PLDPCH-CC constructed by (21). Note that the threshold is slightly lower (i.e., slightly better) than that of the

PLDPCH-BC. We use the lifting factors $z_1 = 32$ and $z_2 = 512$ to expand the protomatrix such that the sub-block length of the SC-PLDPCH-CC equals 1,327,104, which is identical to the code length of the PLDPCH-BC with $z_1 = 32$ and $z_2 = 512$, i.e., $N + M(2^r - r - 2) = 1,327,104$. Moreover, the information length in each sub-block/block is 65536 for both codes. The BER performance of the SC-PLDPCH-CC with different number of processors I used in pipeline decoding is shown in Fig. 6(a). We observe that the decoder with $I = 80$ processors in pipeline decoding achieves a BER of 10^{-5} at about $E_b/N_0 = -1.24$ dB, which outperforms that with (i) $I = 75$ by about 0.015 dB, (ii) $I = 70$ by about 0.03 dB, and (iii) $I = 60$ by about 0.06 dB. The gaps of the SC-PLDPCH-CC (with $I = 80$ and BER of 10^{-5}) to the PEXIT threshold (-1.35 dB) and to the

⁷In [16], (15) has been used to compute I_{eh} . It is not very efficient because of the need to evaluate the PDF of the LLR values. In this paper, (16) is used instead to compute I_{eh} because it can be evaluated much more efficiently with graphics processing units. The computed thresholds are found to be slightly different and larger than those reported in [16].

ultimate Shannon limit (-1.59 dB) are about 0.11 dB and 0.35 dB, respectively.

In the same figure, we plot the BER results of the underlying PLDPCH-BC using $I_{max} = 300$ standard decoding iterations, which should achieve almost the same BER performance as $I_{max}/2 = 150 = I_{BC}$ layered decoding iterations [20]. We recall in Sect. IV-C2 that when $(W+1)I = I_{BC}$, the latencies of both SC-PLDPCH-CC pipeline decoder and PLDPCH-BC decoder become identical. Thus when $I_{BC} = 150$ layered decoding iterations are used in the PLDPCH-BC decoder, the number of processors used in the SC-PLDPCH-CC pipeline decoder equals $I = 150/(W+1) = 75$. Comparing the corresponding BER curves in the figure shows that the SC-PLDPCH-CC outperforms the PLDPCH-BC by about 0.04 dB at a BER of 10^{-5} . Next, we increase the second lifting factor of the PLDPCH-BC by a factor of $\delta_{z_2} = 1 + \frac{W}{1+(2^r-r-2)\frac{m}{n}} = 1.136$ such that the blocklength of the PLDPCH-BC is the same as constraint length of the SC-PLDPCH-CC. Thus the second lifting factor of the PLDPCH-BC becomes $z'_2 = 512 \times 1.136 \approx 582$. To maintain the same decoding latency, the number of layered iterations is reduced from $I_{BC} = 150$ to $I'_{BC} = I_{BC}/\delta_{z_2} = 150/1.136 = 132$. In other words, $I_{max} = 300$ is reduced to $I'_{max} = 300/1.136 \approx 264$. Comparing the BER curves in the figure shows that under the same constraint length/blocklength and the same decoding latency, the SC-PLDPCH-CC outperforms the PLDPCH-BC by about 0.03 dB at a BER of 10^{-5} .

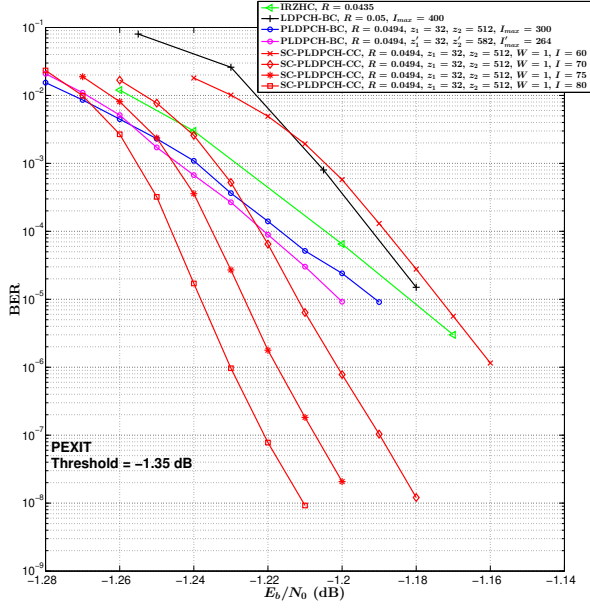
We further compare our proposed code with the rate-0.0453 irregular zigzag-Hadamard code (IRZHC) [45], the rate-0.05 LDPC-Hadamard block code (LDPCH-BC) [14] and the rate-0.033 turbo-Hadamard code (THC) [9], [14]. To have a fair comparison, the information lengths in each block are about 65536 for all codes. First, it is given in [14, Fig. 10] that the rate-0.033 THC (with 80 iterations) achieves a BER of 10^{-5} at $E_b/N_0 = -0.95$ dB. In Fig. 6, we further redraw the BER curves of IRZHC ([45, Fig. 12]) and LDPCH-BC ([14, Fig. 10]). As can be observed, IRZHC and LDPCH-BC (with $I_{max} = 400$ standard decoding iterations) achieve a BER of 10^{-5} at $E_b/N_0 = -1.17$ dB and -1.18 dB, respectively. However, our SC-PLDPCH-CC (using pipeline decoder with 80 processors) can attain the same BER at $E_b/N_0 = -1.238$ dB. Finally, we use

the lifting factors $z_1 = 32$ and $z_2 = 4$ to expand the protomatrix such that the sub-block length of the SC-PLDPCH-CC equals 10368 . Fig. 6(b) plots the BER results of the code. At $I = 80$ and a BER of 10^{-5} , the SC-PLDPCH-CC degrades from -1.24 dB to -0.85 dB when the sub-block length is reduced from $1,327,104$ to 10368 .

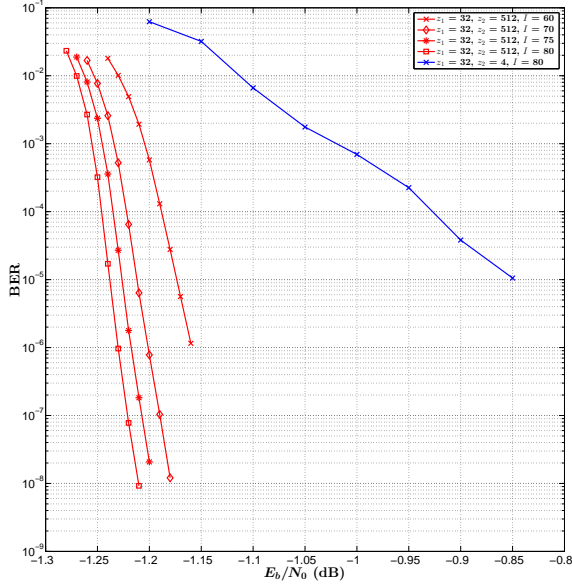
B. Rate-0.021 and $r = 5$

Based on the 6×10 protomatrix of the optimized rate-0.021 PLDPCH-BC [16], we apply GA and find the 6×10 protomatrices shown as (22) after 50 generations. The corresponding fitness value equals 609. Using the proposed layered PEXIT method, Table II lists the thresholds for the $r = 5$ SC-PLDPCH-TDC constructed by (22) and for the $r = 5$ PLDPCH-BC [16]. The theoretical threshold of the SC-PLDPCH-TDC with $L = 300$ is estimated to be -1.37 dB, which is the same with that of the PLDPCH-BC [16]. Hence, we consider that the $r = 5$ SC-PLDPCH-CC constructed by (22) has a threshold of about -1.37 dB. We use the same lifting factors, i.e., $z_1 = 32$ and $z_2 = 512$, as those used in the PLDPCH-BC to expand the protomatrix such that the sub-block length of the SC-PLDPCH-CC equals $3,112,960$. The information length in each sub-block/block is 65536 for both codes.

The BER performance of the SC-PLDPCH-CC with different I is shown in Fig. 7. The pipeline decoder with $I = 80$ processors achieves a BER of 10^{-5} at about $E_b/N_0 = -1.30$ dB, which outperforms that with (i) $I = 75$ by about 0.01 dB, (ii) $I = 70$ by about 0.02 dB, and (iii) $I = 60$ by about 0.05 dB. The gaps of the SC-PLDPCH-CC (with $I = 80$ and BER of 10^{-5}) to the PEXIT threshold (-1.37 dB) and to the ultimate Shannon limit (-1.59 dB) are about 0.07 dB and 0.29 dB, respectively. In the same figure, we can also observe that under the same latency, SC-PLDPCH-CC using $I = 75$ processors outperforms PLDPCH-BC using $I_{BC} = 150$ layered decoding iterations (equivalent to $I_{max} = 300$ standard decoding iterations, i.e., the blue curve with symbol “o”) by about 0.05 dB at a BER of 10^{-5} . Next, we increase the second lifting factor of the PLDPCH-BC by a factor of $\delta_{z_2} = 1 + \frac{W}{1+(2^r-r-2)\frac{m}{n}} = 1.053$ such that the blocklength of the PLDPCH-BC is the same as constraint length of the SC-PLDPCH-CC. Thus the second lifting factor of the PLDPCH-BC equals



(a)



(b)

Fig. 6. (a) BER performance of rate-0.0494 SC-PLDPCH-CC (PEXIT threshold = -1.35 dB), rate-0.0494 PLDPCH-BC [16], rate-0.0435 IRZHC [45] and rate-0.05 LDPCH-BC [14]. Information lengths are around 65536 for all codes. $r = 4$, lifting factors $z_1 = 32$ and $z_2 = 512$ for SC-PLDPCH-CC. $r = 4$, lifting factor sets (i) $z_1 = 32$ and $z_2 = 512$; and (ii) $z'_1 = 32$ and $z'_2 = 582$ for PLDPCH-BC. (b) BER performance of rate-0.0494 SC-PLDPCH-CC with different sub-block lengths.

$z'_2 = 512 \times \delta_{z_2} = 512 \times 1.053 = 539$. To maintain the same decoding latency, $I'_{BC} = I_{BC}/\delta_{z_2} = 150/1.053 \approx 142$ and $I'_{max} = I_{max}/1.053 \approx 284$.

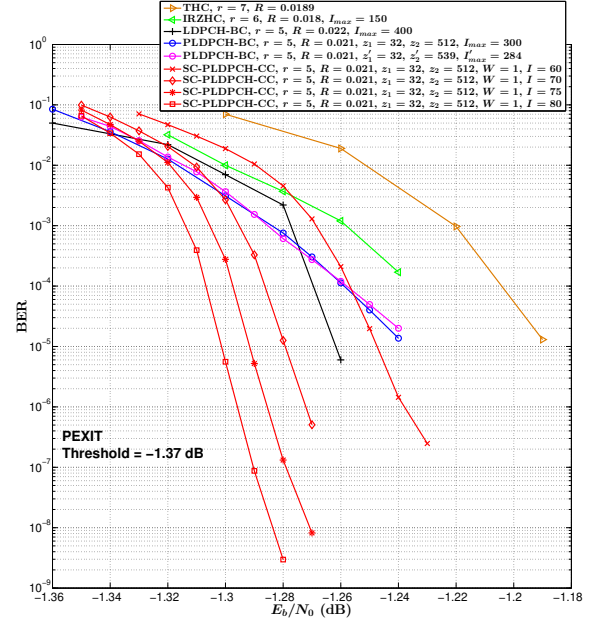


Fig. 7. BER performance of rate-0.021 SC-PLDPCH-CC (PEXIT threshold = -1.37 dB), rate-0.021 PLDPCH-BC [16], rate-0.0189 THC [9], rate-0.018 IRZHC [46] and rate-0.022 LDPCH-BC [14]. Information lengths are around 65536 for all codes. $r = 5$, lifting factors $z_1 = 32$ and $z_2 = 512$ for SC-PLDPCH-CC. $r = 5$, lifting factor sets (i) $z_1 = 32$ and $z_2 = 512$; and (ii) $z'_1 = 32$ and $z'_2 = 539$ for PLDPCH-BC.

Comparing the BER curves in the figure shows that under the same constraint length/blocklength and the same decoding latency, the SC-PLDPCH-CC outperforms the PLDPCH-BC by more than 0.05 dB at a BER of 10^{-5} .

In Fig. 7, we further redraw the BER curves of rate-0.0189 THC [9, Fig. 11], rate-0.018 IRZHC [46, Fig. 14] and rate-0.022 LDPCH-BC [14, Fig. 12]. To have a fair comparison, the information lengths in each block are about 65536 for all codes. At a BER of 10^{-5} , THC, IRZHC (with $I_{max} = 150$ iterations) and LDPCH-BC (with $I_{max} = 400$ iterations) require E_b/N_0 values of -1.17 dB, -1.24 dB and -1.26 dB, respectively; while our rate-0.021 SC-PLDPCH-CC using the pipeline decoding with $I = 80$ processors requires only $E_b/N_0 = -1.30$ dB.

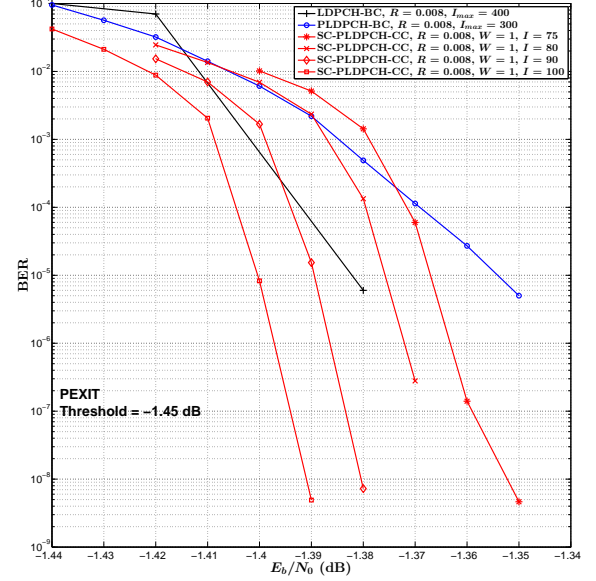
C. Rate-0.008 and $r = 8$, Rate-0.00295 and $r = 10$

Based on the 5×15 protomatrix \mathbf{B} of the optimized rate-0.008 PLDPCH-BC [16], we apply our proposed GA and find the protomatrices shown as (23) and (24). The protomatrices are found after

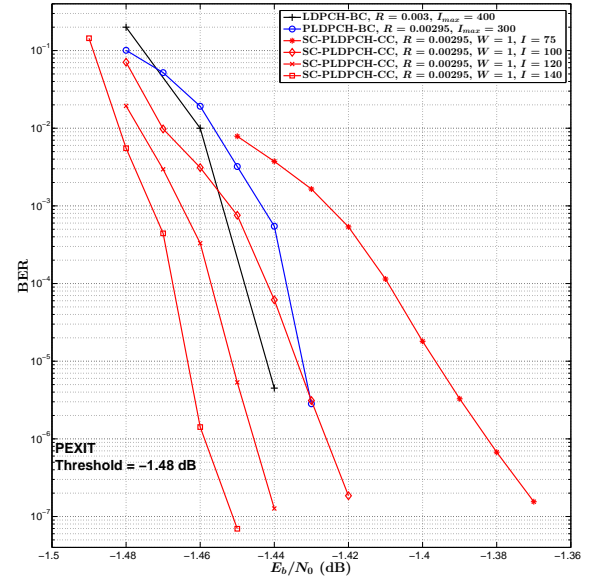
59 generations and the corresponding fitness value equals 457. We increase L to 300 such that the SC-PLDPCH-TDC has the same code rate with its underlying block code [16]. Using our proposed PEXIT method, the terminated code with $L = 300$ has a threshold of -1.45 dB as shown in Table II. Hence, the theoretical threshold of the SC-PLDPCH-CC constructed by (23) and (24) approximately equals -1.45 dB, which is slightly lower (i.e., slightly better) than that of the PLDPCH-BC [16]. We lift the SC-PLDPCH-CC with factors $z_1 = 16$ and $z_2 = 1280$ such that its sub-block length is the same as that of the PLDPCH-BC in [16]. Moreover, the information lengths in each sub-block/block equal 204800 for both codes.

Fig. 8(a) shows the BER performance of the two codes. An SC-PLDPCH-CC pipeline decoder with $I = 100$ processors achieves a BER of 10^{-5} at about $E_b/N_0 = -1.40$ dB, which outperforms that with (i) $I = 90$ by about 0.01 dB, (ii) $I = 80$ by about 0.025 dB, (iii) and $I = 75$ by about 0.035 dB. The gaps of the SC-PLDPCH-CC (with $I = 100$ and BER of 10^{-5}) to the PEXIT threshold (-1.45 dB) and to the ultimate Shannon limit (-1.59) dB are 0.05 dB and 0.19 dB, respectively. We can also observe that under the same latency, SC-PLDPCH-CC using $I = 75$ processors outperforms PLDPCH-BC using $I_{BC} = 150$ layered decoding iterations (equivalent to $I_{max} = 300$ standard decoding iterations, i.e., the blue curve with symbol “o”) by about 0.01 dB at a BER of 10^{-5} . In Fig. 8(a), we re-draw the BER curve of rate-0.008 LDPCH-BC [14, Fig. 13] which has an information length of 238000. We see that at a BER of 10^{-5} , the required E_b/N_0 for the rate-0.008 LDPCH-BC (with $I_{max} = 400$ iterations) is -1.38 dB and that for our rate-0.008 SC-PLDPCH-CC (pipeline decoder containing 100 processors) is -1.40 dB.

Based on the 6×24 protomatrix \mathbf{B} of the optimized rate-0.00295 PLDPCH-BC [16], the two protomatrices \mathbf{B}_0 and \mathbf{B}_1 obtained by our proposed GA are shown in (25) and (26), respectively. The protomatrices (25) and (26) are found after 48 generations, and the corresponding fitness value equals 516. Using the proposed PEXIT method, Table II lists the thresholds for SC-PLDPCH-TDC with $L = 100$ and the underlying PLDPCH-BC [16]. The SC-PLDPCH-TDC constructed by $L = 100$ sets of protomatrices (25) and (26) has almost the same code rate with its underlying block code, and



(a)



(b)

Fig. 8. (a) BER performance of rate-0.008 SC-PLDPCH-CC (PEXIT threshold = -1.45 dB), rate-0.008 PLDPCH-BC [16] and rate-0.008 LDPCH-BC [14]. Information length is 204,800 for both SC-PLDPCH-CC and PLDPCH-BC; and 238,000 for LDPCH-BC. $r = 8$, lifting factors $z_1 = 16$ and $z_2 = 1,280$ for both SC-PLDPCH-CC and PLDPCH-BC. (b) BER performance of rate-0.00295 SC-PLDPCH-CC (PEXIT threshold = -1.48 dB), rate-0.00295 PLDPCH-BC [16] and rate-0.003 LDPCH-BC [14]. Information length is 460,800 for both SC-PLDPCH-CC and PLDPCH-BC; and 650,00 for LDPCH-BC. $r = 10$, lifting factors $z_1 = 20$ and $z_2 = 1,280$ for both SC-PLDPCH-CC and PLDPCH-BC.

its threshold is estimated to be -1.48 dB. Hence, the theoretical threshold of the SC-PLDPCH-CC constructed by (25) and (26) also equals -1.48 dB, which is slightly greater than that of the PLDPCH-BC [16]. We lift the SC-PLDPCH-CC with factors $z_1 = 20$ and $z_2 = 1280$ such that its sub-block length is the same as that of the PLDPCH-BC [16]. Fig. 8(b) shows the BER performance of the two codes. SC-PLDPCH-CC decoder with $I = 140$ processors achieves a BER of 10^{-5} at about $E_b/N_0 = -1.465$ dB, which outperforms that with (i) $I = 120$ by about 0.01 dB, (ii) $I = 100$ by about 0.03 dB, and (iii) $I = 75$ by about 0.07 dB. At a BER of 10^{-5} , the gaps (for the SC-PLDPCH-CC with $I = 140$ iterations) to the PEXIT threshold (-1.48 dB) and to the ultimate Shannon limit (-1.59 dB) are 0.015 dB and 0.125 dB, respectively. Under the same latency, SC-PLDPCH-CC using $I = 75$ processors is outperformed by PLDPCH-BC using $I_{BC} = 150$ layered decoding iterations (equivalent to $I_{max} = 300$ standard decoding iterations) by about 0.04 dB at a BER of 10^{-5} .

In Fig. 8(b), we redraw the BER curve of rate-0.003 LDPCH-BC [14, Fig. 13] which has an information length of 650,000. Results show that the rate-0.003 LDPCH-BC (with $I_{max} = 400$ iterations) achieves a BER of 10^{-5} at $E_b/N_0 = -1.44$ dB and the rate-0.00295 SC-PLDPCH-CC (containing $I = 140$ processors) achieves the same error performance at $E_b/N_0 = -1.465$ dB.

VI. CONCLUSION

We have proposed a new type of ultimate-Shannon-limit-approaching code called SC-PLDPCH-CCs, which are formed by spatially coupling PLDPCH-BCs. We have developed a pipelined decoding with layered scheduling algorithm to efficiently and effectively decode SC-PLDPCH-CCs, and have proposed a layered PEXIT method to evaluate the threshold of SC-PLDPCH-TDCs. Based on the protomatrix of a PLDPCH-BC, we have proposed a genetic algorithm to systematically search for the protomatrices of good SC-PLDPCH-TDCs. We extend the coupling length of these SC-PLDPCH-TDCs with good thresholds to form SC-PLDPCH-CCs. Using the proposed methods, we have found SC-PLDPCH-CCs which are comparable to or superior to their block code counterparts in terms of theoretical threshold

and error performance. Their simulated error performances outperform state-of-the-art low-rate codes with comparable rates and information lengths. At a BER of 10^{-5} , the SC-PLDPCH-CCs of rates 0.0494, 0.021, 0.008 and 0.00295 are only 0.352 dB, 0.29 dB, 0.19 dB and 0.125 dB from the ultimate Shannon limit.

REFERENCES

- [1] R. G. Gallager, *Low-Density Parity-Check Codes*. PhD thesis, Cambridge, MA, USA, 1963.
- [2] R. M. Tanner, "A recursive approach to low complexity codes," *IEEE Trans. Inf. Theory*, vol. 27, no. 5, pp. 533–547, Sep. 1981.
- [3] T. J. Richardson, M. A. Shokrollahi, and R. L. Urbanke, "Design of capacity-approaching irregular low-density parity-check codes," *IEEE Trans. Inf. Theory*, vol. 47, no. 2, pp. 619–637, Feb. 2001.
- [4] S. T. Brink, G. Kramer, and A. Ashikhmin, "Design of low-density parity-check codes for modulation and detection," *IEEE Trans. Commun.*, vol. 52, no. 4, pp. 670–678, Apr. 2004.
- [5] E. Sharon, A. Ashikhmin, and S. Litsyn, "Analysis of low-density parity-check codes based on EXIT functions," *IEEE Trans. Commun.*, vol. 54, no. 8, pp. 1407–1414, 2006.
- [6] D. J. Costello and G. D. Forney, "Channel coding: The road to channel capacity," *Proc. IEEE*, vol. 95, no. 6, pp. 1150–1177, 2007.
- [7] L. Ping, L. Liu, K. Y. Wu, and W. K. Leung, "Approaching the capacity of multiple access channels using interleaved low-rate codes," *IEEE Commun. Lett.*, vol. 8, no. 1, pp. 4–6, 2004.
- [8] L. Ping, L. Liu, K. Wu, and W. Leung, "Interleave division multiple-access," *IEEE Trans. Wireless Commun.*, vol. 5, no. 4, pp. 938–947, 2006.
- [9] L. Ping, W. K. Leung, and K. Y. Wu, "Low-rate turbo-Hadamard codes," *IEEE Trans. Inf. Theory*, vol. 49, no. 12, pp. 3213–3224, Dec. 2003.
- [10] W. K. R. Leung, G. Yue, L. Ping, and X. Wang, "Concatenated zigzag Hadamard codes," *IEEE Trans. Inf. Theory*, vol. 52, no. 4, pp. 1711–1723, 2006.
- [11] S. Jiang, P. W. Zhang, F. C. M. Lau, C.-W. Sham, and K. Huang, "A turbo-Hadamard encoder/decoder system with hundreds of Mbps throughput," in *2018 IEEE 10th Int. Symp. Turbo Codes Iterative Inf. Process. (ISTC)*, pp. 1–5, 2018.
- [12] S. Jiang, P. W. Zhang, F. C. M. Lau, and C.-W. Sham, "An ultimate-Shannon-limit-approaching Gbps throughput encoder/decoder system," *IEEE Trans. Circuits Syst. II, Exp. Briefs*, vol. 67, no. 10, pp. 2169–2173, 2020.
- [13] S. Jiang, F. C. M. Lau, and C.-W. Sham, "Hardware design of concatenated zigzag Hadamard encoder/decoder system with high throughput," *IEEE Access*, vol. 8, pp. 165298–165306, 2020.
- [14] G. Yue, L. Ping, and X. Wang, "Generalized low-density parity-check codes based on Hadamard constraints," *IEEE Trans. Inf. Theory*, vol. 53, no. 3, pp. 1058–1079, 2007.
- [15] X. Y. Hu, E. Eleftheriou, and D. M. Arnold, "Regular and irregular progressive edge-growth Tanner graphs," *IEEE Trans. Inf. Theory*, vol. 51, no. 1, pp. 386–398, Jan. 2005.
- [16] P.-W. Zhang, F. C. M. Lau, and C.-W. Sham, "Protograph-based LDPC Hadamard codes," *IEEE Trans. Commun.*, vol. 69, no. 8, pp. 4998–5013, 2021.
- [17] J. Thorpe, "Low-density parity-check (LDPC) codes constructed from protographs," in *Proc. IPN Progr. Rep.*, pp. 1–7, Aug. 2003.

- [18] M. Fossorier, "Quasi-cyclic low-density parity-check codes from circulant permutation matrices," *IEEE Trans. Inf. Theory*, vol. 50, no. 8, pp. 1788–1793, Aug. 2004.
- [19] G. Liva and M. Chiani, "Protograph LDPC codes design based on EXIT analysis," *IEEE GLOBECOM 2007*, pp. 3250–3254, 2007.
- [20] P. W. Zhang, F. C. M. Lau, and C.-W. Sham, "Layered decoding for protograph-based low-density parity-check Hadamard codes," *IEEE Commun. Lett.*, vol. 25, no. 6, pp. 1776–1780, 2021.
- [21] A. R. Iyengar, M. Papaleo, P. H. Siegel, J. K. Wolf, A. Vanelli-Coralli, and G. E. Corazza, "Windowed decoding of protograph-based LDPC convolutional codes over erasure channels," *IEEE Trans. Inf. Theory*, vol. 58, no. 4, pp. 2303–2320, 2012.
- [22] A. Jimenez Felstrom and K. Zigangirov, "Time-varying periodic convolutional codes with low-density parity-check matrix," *IEEE Trans. Inf. Theory*, vol. 45, no. 6, pp. 2181–2191, 1999.
- [23] S. Kudekar, T. J. Richardson, and R. L. Urbanke, "Threshold saturation via spatial coupling: Why convolutional LDPC ensembles perform so well over the BEC," *IEEE Trans. Inf. Theory*, vol. 57, no. 2, pp. 803–834, 2011.
- [24] S. Kudekar, T. Richardson, and R. L. Urbanke, "Spatially coupled ensembles universally achieve capacity under belief propagation," *IEEE Trans. Inf. Theory*, vol. 59, no. 12, pp. 7761–7813, 2013.
- [25] M. Stinner and P. M. Olmos, "On the waterfall performance of finite-length SC-LDPC codes constructed from protographs," *IEEE J. Sel. Areas Commun.*, vol. 34, no. 2, pp. 345–361, 2016.
- [26] M. Battaglioni, M. Baldi, and E. Paolini, "Complexity-constrained spatially coupled LDPC codes based on protographs," in *Proc. 2017 Int. Symp. Wireless Commun. Syst. (ISWCS)*, pp. 49–53, 2017.
- [27] L. Wei, D. G. M. Mitchell, T. E. Fuja, and D. J. Costello, "Design of spatially coupled LDPC codes over GF(q) for windowed decoding," *IEEE Transactions on Information Theory*, vol. 62, no. 9, pp. 4781–4800, 2016.
- [28] M. Srinivas and L. M. Patnaik, "Genetic algorithms: A survey," *Computer*, vol. 27, no. 6, pp. 17–26, 1994.
- [29] L. Hebbes, R. Malyan, and A. Lenaghan, "Genetic algorithms for turbo codes," in *Proc. The Int. Conf. "Computer as a Tool"*, vol. 1, pp. 478–481, 2005.
- [30] A. Elkelesh, M. Ebada, S. Cammerer, and S. T. Brink, "Decoder-tailored polar code design using the genetic algorithm," *IEEE Trans. Commun.*, vol. 67, no. 7, pp. 4521–4534, 2019.
- [31] A. Elkelesh, M. Ebada, S. Cammerer, L. Schmalen, and S. T. Brink, "Decoder-in-the-loop: Genetic optimization-based LDPC code design," *IEEE Access*, vol. 7, pp. 141161–141170, 2019.
- [32] Y. Koganei, M. Yofune, C. Li, T. Hoshida, and Y. Amezawa, "SC-LDPC code with nonuniform degree distribution optimized by using genetic algorithm," *IEEE Commun. Lett.*, vol. 20, no. 5, pp. 874–877, 2016.
- [33] Y. Liao, M. Qiu, and J. Yuan, "Design and analysis of delayed bit-interleaved coded modulation with ldpc codes," *IEEE Transactions on Communications*, vol. 69, no. 6, pp. 3556–3571, 2021.
- [34] Y. Liao, M. Qiu, and J. Yuan, "Connecting spatially coupled ldpc code chains for bit-interleaved coded modulation," in *2021 11th International Symposium on Topics in Coding (ISTC)*, pp. 1–5, 2021.
- [35] Y. Wang, S. C. Draper, and J. S. Yedidia, "Hierarchical and high-girth QC LDPC codes," *IEEE Trans. Inf. Theory*, vol. 59, no. 7, pp. 4553–4583, 2013.
- [36] D. G. M. Mitchell, M. Lentmaier, and D. J. Costello, "Spatially coupled LDPC codes constructed from protographs," *IEEE Trans. Inf. Theory*, vol. 61, no. 9, pp. 4866–4889, 2015.
- [37] M. Battaglioni, F. Chiaraluce, M. Baldi, and M. Lentmaier, "Girth analysis and design of periodically time-varying SC-LDPC codes," *IEEE Trans. Inf. Theory*, vol. 67, no. 4, pp. 2217–2235, 2021.
- [38] D. J. Costello, L. Dolecek, T. E. Fuja, J. Kliewer, D. G. Mitchell, and R. Smarandache, "Spatially coupled sparse codes on graphs: Theory and practice," *IEEE Commun. Mag.*, vol. 52, no. 7, pp. 168–176, 2014.
- [39] C.-W. Sham, X. Chen, F. C. M. Lau, Y. Zhao, and W. M. Tam, "A 2.0 Gb/s throughput decoder for QC-LDPC convolutional codes," *IEEE Trans. Circuits Syst. I, Reg. Papers*, vol. 60, no. 7, pp. 1857–1869, 2013.
- [40] P. W. Zhang, F. C. M. Lau, and C.-W. Sham, "Hardware architecture of layered decoders for PLDPC-Hadamard codes," <https://arxiv.org/abs/2110.07906>, 2021.
- [41] Y. Fang, G. A. Bi, Y. L. Guan, and F. C. M. Lau, "A survey on protograph LDPC codes and their applications," *IEEE Commun. Surv. Tut.*, vol. 17, no. 4, pp. 1989–2016, 2015.
- [42] S. T. Brink, "Convergence behavior of iteratively decoded parallel concatenated codes," *IEEE Trans. Commun.*, vol. 49, no. 10, pp. 1727–1737, Oct. 2001.
- [43] Z. Yang, Y. Fang, G. Cai, G. Zhang, and P. Chen, "Design and optimization of tail-biting spatially coupled protograph LDPC codes under shuffled belief-propagation decoding," *IEEE Commun. Lett.*, vol. 24, no. 7, pp. 1378–1382, 2020.
- [44] J. H. Holland, *Adaptation in Natural and Artificial System*. Univ. of Michigan Press, Ann Arbor, 1975.
- [45] K. Li, X. Wang, and A. Ashikhmin, "EXIT functions of Hadamard components in repeat-zigzag-Hadamard (RZH) codes with parallel decoding," *IEEE Trans. Inf. Theory*, vol. 54, no. 4, pp. 1773–1785, 2008.
- [46] K. Li, G. Yue, X. Wang, and L. Ping, "Low-rate repeat-zigzag-Hadamard codes," *IEEE Trans. Inf. Theory*, vol. 54, no. 2, pp. 531–543, 2008.



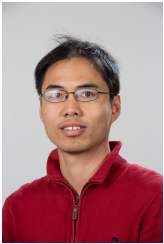
Peng-Wei Zhang received the Bachelor of Engineering degree in Electronics and Information Engineering and the Master of Engineering degree in Electronics and Communication Engineering from Chongqing University of Posts and Telecommunications, China, in 2013 and 2016, respectively. He received his PhD degree at the Department of Electronic and Information Engineering, The Hong Kong Polytechnic University, Hong Kong SAR, China, in 2021. He is now with Huawei Technologies Ltd., Chengdu, China.



Francis C. M. Lau received the BEng(Hons) degree in electrical and electronic engineering and the PhD degree from King's College London, University of London, UK. He is a Professor at the Department of Electronic and Information Engineering, The Hong Kong Polytechnic University, Hong Kong. He is also a Fellow of IEEE and a Fellow of IET.

He is a co-author of two research monographs. He is also a co-holder of six US patents. He has published more than 330 papers. His main research interests include channel coding, cooperative networks, wireless sensor networks, chaos-based digital communications, applications of complex-network theories, and wireless communications. He is a co-recipient of one Natural Science Award from the Guangdong Provincial Government, China; eight best/outstanding conference paper awards; one technology transfer award; two young scientist awards from International Union of Radio Science; and one FPGA design competition award.

He was the General Co-chair of International Symposium on Turbo Codes & Iterative Information Processing (2018) and the Chair of Technical Committee on Nonlinear Circuits and Systems, IEEE Circuits and Systems Society (2012-13). He served as an associate editor for IEEE TRANSACTIONS ON CIRCUITS AND SYSTEMS II (2004-2005 and 2015-2019), IEEE TRANSACTIONS ON CIRCUITS AND SYSTEMS I (2006-2007), and IEEE CIRCUITS AND SYSTEMS MAGAZINE (2012-2015). He has been a guest associate editor of INTERNATIONAL JOURNAL AND BIFURCATION AND CHAOS since 2010.



Chiu-Wing Sham received his Bachelor degree (Computer Engineering) and MPhil. degree from The Chinese University of Hong Kong in 2000 and 2002 respectively, and received his Ph.D. degree from the same university in 2006. He has worked as an Electronic Engineer on the FPGA applications of the motion-control system and system security with cryptography in ASM Pacific Technology

Ltd (HK). During the years at The Hong Kong Polytechnic University, he engaged in various University projects for the commercialization of technology, in particular, a few optical communication projects which were in collaboration with Huawei. He also worked on the physical design of VLSI design automation. He was invited to work at Synopsys, Inc. (Shanghai) in the summer of 2005 as a Visiting Research Engineer. He is now working at The University of Auckland as a Senior Lecturer. He is also an IEEE Senior Member and an Associate Editor of IEEE TRANSACTIONS ON CIRCUITS AND SYSTEMS II (2017-present).